

University of New Hampshire

## University of New Hampshire Scholars' Repository

---

Faculty Publications

---

7-21-2020

### Fine particle pH and sensitivity to NH<sub>3</sub> and HNO<sub>3</sub> over summertime South Korea during KORUS-AQ

Ifayoyinsola Ibikunle  
*Georgia Institute of Technology*

Andreas Beyersdorf  
*NASA Langley Research Center*

Pedro Campuzano-Jost  
*University of Colorado*

Chelsea Corr  
*NASA Langley Research Center*

John D. Crouse  
*California Institute of Technology*

*See next page for additional authors*

Follow this and additional works at: [https://scholars.unh.edu/faculty\\_pubs](https://scholars.unh.edu/faculty_pubs)

---

#### Recommended Citation

Ibikunle, I., A. Beyersdorf, P. Campuzano-Jost, C. Corr, J. D. Crouse, J. Dibb, G. Diskin, G. Huey, J.-L. Jimenez, M. J. Kim, B. A. Nault, E. Scheuer, A. Teng, P. O. Wennberg, B. Anderson, J. Crawford, R. Weber, and A. Nenes (2020), Fine particle pH and sensitivity to NH<sub>3</sub> and HNO<sub>3</sub> over summertime South Korea during KORUS-AQ, *Atmospheric Chemistry and Physics Discussion*.

This Article is brought to you for free and open access by University of New Hampshire Scholars' Repository. It has been accepted for inclusion in Faculty Publications by an authorized administrator of University of New Hampshire Scholars' Repository. For more information, please contact [Scholarly.Communication@unh.edu](mailto:Scholarly.Communication@unh.edu).

---

**Authors**

Ifayoyinsola Ibikunle, Andreas Beyersdorf, Pedro Campuzano-Jost, Chelsea Corr, John D. Crouse, Jack E. Dibb, Glenn Diskin, Greg Huey, Jose-Luis Jimenez, Michelle J. Kim, Benjamin A. Nault, Eric Scheuer, Alex Teng, Paul O. Wennberg, Bruce Anderson, James Crawford, Rodney Weber, and Athanasios Nenes



1 **Fine particle pH and sensitivity to NH<sub>3</sub> and HNO<sub>3</sub> over summertime South Korea during**  
2 **KORUS-AQ**

3 Ifayoyinsola Ibikunle<sup>1</sup>, Andreas Beyersdorf<sup>2</sup>, Pedro Campuzano-Jost<sup>3,4</sup>, Chelsea Corr<sup>2+</sup>, John D.  
4 Crouse<sup>5</sup>, Jack Dibb<sup>6</sup>, Glenn Diskin<sup>7</sup>, Greg Huey<sup>8</sup>, Jose-Luis Jimenez<sup>3,4</sup>, Michelle J. Kim<sup>5</sup>,  
5 Benjamin A. Nault<sup>3,4</sup>, Eric Scheuer<sup>6</sup> Alex Teng<sup>5</sup>, Paul O. Wennberg<sup>5</sup>, Bruce Anderson<sup>2</sup>, James  
6 Crawford<sup>2</sup>, Rodney Weber<sup>\*8</sup>, Athanasios Nenes<sup>\*8,9,10</sup>

7

8 <sup>1</sup>School of Chemical and Biomolecular Engineering, Georgia Institute of Technology, Atlanta, GA  
9 30332, USA

10 <sup>2</sup>NASA Langley Research Center, Hampton, VA 23681, USA

11 <sup>3</sup>Department of Chemistry, University of Colorado, Boulder, CO 80309, USA

12 <sup>4</sup>Cooperative Institute for Research in Environmental Sciences, University of Colorado, Boulder,  
13 CO 80309, USA

14 <sup>5</sup>California Institute of Technology, Pasadena, CA 91125

15 <sup>6</sup>Institute for the Study of Earth, Oceans, and Space, University of New Hampshire, Durham, NH  
16 03824, USA

17 <sup>7</sup>NASA Ames Research Center, Moffett Field, CA 94035, USA

18 <sup>8</sup>School of Earth and Atmospheric Sciences, Georgia Institute of Technology, Atlanta, GA 30332,  
19 USA

20 <sup>9</sup>School of Architecture, Civil & Environmental Engineering, Ecole Polytechnique Fédérale de  
21 Lausanne, CH-1015, Lausanne, Switzerland

22 <sup>10</sup>Center for the Study of Air Quality and Climate Change, Institute for Chemical Engineering  
23 Sciences, Foundation for Research and Technology Hellas, Patras, GR-26504, Greece

24 <sup>+</sup>Currently at Colorado State University

25

26 \*correspondence to [athanasios.nenes@epfl.ch](mailto:athanasios.nenes@epfl.ch) and [rweber@eas.gatech.edu](mailto:rweber@eas.gatech.edu)

27



## 28 **Abstract**

29 Using a new approach that constrains thermodynamic modeling of aerosol composition with  
30 measured gas-to-particle partitioning of inorganic nitrate, we estimate the acidity levels for aerosol  
31 sampled in the South Korean planetary boundary layer during the NASA/NIER KORUS-AQ field  
32 campaign. The pH (mean  $\pm 1\sigma = 2.43 \pm 0.68$ ) and aerosol liquid water content determined were then  
33 used to determine the “chemical regime” of the inorganic fraction of particulate matter (PM)  
34 sensitivity to ammonia and nitrate availability. We found that the aerosol formation is always  
35 sensitive to  $\text{HNO}_3$  levels, especially in highly polluted regions, while it is only exclusively  
36 sensitive to  $\text{NH}_3$  in some rural/remote regions. Nitrate levels are further promoted because dry  
37 deposition velocity is low and allows its accumulation in the boundary layer. Because of this,  
38  $\text{HNO}_3$  reductions achieved by  $\text{NO}_x$  controls prove to be the most effective approach for all  
39 conditions examined, and that  $\text{NH}_3$  emissions can only partially affect PM reduction for the  
40 specific season and region. Despite the benefits of controlling PM formation to reduce ammonium-  
41 nitrate aerosol and PM mass, changes in the acidity domain can significantly affect other processes  
42 and sources of aerosol toxicity (such as e.g., solubilization of Fe, Cu and other metals) as well as  
43 the deposition patterns of these trace species and reactive nitrate.

44

## 45 **1. Introduction**

46 Poor air quality from high concentrations of fine particulate matter over South Korea has its origin  
47 in domestic emissions from vehicles, industry, and biomass burning, combined with long-range  
48 transport of pollutants from mainland China (Kim et al., 2018; Nault et al., 2018). Because air  
49 quality in South Korea is a mixture of factors such as regional and local emissions from both  
50 anthropogenic and natural (e.g. dust) sources, as well as meteorological (e.g. wind, relative



51 humidity) and chemical interactions (e.g. photochemistry), assessing possible air pollution control  
52 strategies in this region is challenging (RSSR, 2016).

53 To improve our understanding of poor air quality in South Korea, the Korean National Institute of  
54 Environmental Research (NIER) and the United States National Aeronautics and Space  
55 Administration (NASA), conducted a field study in South Korea from 26 April to 18 June 2016  
56 (RSSR, 2016). The aim of the Korea-United States Air Quality Study (KORUS-AQ), was to  
57 determine the factors that contribute to the poor regional air quality to aid the development of  
58 effective air quality mitigation strategies.

59 During the KORUS-AQ campaign, secondary production of particulate matter (PM) – organic and  
60 inorganic – constitute a significant fraction of PM pollution, with significant contribution from  
61 local sources. Since sulfate and nitrate comprised nearly half of the mass of PM at sizes smaller  
62 than 1  $\mu\text{m}$  ( $\text{PM}_{1}$ ) (Jordan et al., in review; Nault et al., 2018), aerosol acidity, liquid water content  
63 and temperature will significantly affect aerosol properties including its mass through the gas-  
64 particle partitioning of semi-volatile species (Nenes et al., 2020a). More broadly, fine aerosol  
65 particle acidity in South Korea affects air quality and human health and therefore requires  
66 knowledge of aerosol pH levels (e.g., Nenes et al., 2020a).

67 Given that direct measurement of atmospheric aerosol pH remains a challenge, there is large  
68 uncertainty in this important parameter (Pye et al., 2020). Of all approaches used to date for  
69 constraining aerosol pH, use of thermodynamic analysis of gas-aerosol observations together with  
70 a model provides the most robust estimates of aerosol acidity (Hennigan et al., 2015; Song et al.,  
71 2018; Pye et al., 2020). To achieve the most robust pH predictions, thermodynamic analysis  
72 requires observations of all species, both gas and particle phase, that affect pH. Knowledge of gas-  
73 phase ammonia and particulate ammonium is especially important, owing to its role as the



74 dominant cation in fine-mode aerosol and pH-sensitive partitioning. Accurate measurement of  
75 ammonia, especially at low concentrations, is far from trivial (Zhu et al., 2015; Wang et al., 2015)  
76 and subject to biases from adsorption of  $\text{NH}_3$  in instrument inlets and  $\text{NH}_4^+$  volatilization (Dawson  
77 et al., 2014; Osada 2011; Yokelson et al., 2003; Guo et al., 2018a). Although measurements of  
78 aerosol  $\text{NH}_4^+$  are common, gas-phase measurements of  $\text{NH}_3$  are often missing in field studies –  
79 including for KORUS-AQ. There is a need to accurately infer aerosol pH in the absence of gas-  
80 phase  $\text{NH}_3$  data.

81 This study aims to accurately determine fine particle pH for aerosol in South Korea, and use this  
82 inferred pH to understand the sensitivity of PM mass to the availability of ammonia and nitric acid  
83 (which are two major aerosol precursors). Focusing only on the inorganic fraction of the aerosol,  
84 we develop a computationally rigorous approach to estimate aerosol pH and particle liquid water  
85 despite missing gas-phase ammonia data and apply it to the KORUS-AQ dataset. We then utilize  
86 these data to assess optimal strategies to control inorganic aerosol mass through reduction of either  
87 available nitric acid or ammonia, based on the new approach of Nenes et al. (2020a).

88

## 89 **2. Methods**

### 90 **2.1 Instrumentation**

#### 91 *Non-refractory $\text{PM}_1$ composition*

92 The CU-Boulder highly-customized Aerodyne high-resolution time-of-flight aerosol mass  
93 spectrometer (HR-ToF-AMS) measured non-refractory (NR)  $\text{PM}_1$  composition, including  
94 ammonium, nitrate, sulfate, chloride, and organic aerosol. The basic concept, operation, and  
95 aircraft deployment of the AMS has been described elsewhere (DeCarlo et al., 2006, 2008; Dunlea  
96 et al., 2009; Kimmel et al., 2011) and the deployment for KORUS-AQ is discussed in detail by



97 Nault et al. (2018). Observations are reported in units of  $\mu\text{g sm}^{-3}$  (under standard conditions of  
98  $T=273.15\text{ K}$ ,  $p=1013\text{ hPa}$ ). For the following analysis, the data were converted to concentrations  
99 at ambient conditions for the thermodynamic calculations.

100 The AMS also separately measures the contribution of amines, organonitrates and organosulfates  
101 (Fry et al., 2019; Farmer et al., 2010; Chen et al., 2019). During the campaign, organic nitrates  
102 comprised roughly 8% of the AMS particulate  $\text{NO}_3$  signal and were only an important contribution  
103 to the signal when  $\text{NO}_3$  was below  $0.50\ \mu\text{g sm}^{-3}$  ( $0.45\ \mu\text{g m}^{-3}$ ) (Nault et al., 2018). Average  
104 concentration of nitrate during the campaign was  $8.09 \pm 6.16\ \mu\text{g m}^{-3}$ , so we consider AMS nitrate  
105 to be approximately equal to inorganic aerosol  $\text{NO}_3^-$ . Accuracy ( $2\sigma$ ) for AMS detection of  
106 inorganic species is estimated to be 35% (Bahreini et al, 2009).

#### 107 *Gas-phase HCl and HNO<sub>3</sub>*

108 HCl and HNO<sub>3</sub> measurements were made using the Georgia Institute of Technology Chemical  
109 Ionization Mass Spectrometer (GT CIMS) and the California Institute of Technology CIMS (CIT  
110 CIMS), respectively. The GT CIMS technique utilizes a low-pressure ion source/reactor and  $\text{SF}_6^-$   
111 reagent ion chemistry to detect HCl (Huey et al., 2004; Slusher et al., 2004, Kim et al., 2007). The  
112 CIT CIMS utilizes  $\text{CF}_3\text{O}^-$  chemistry to detect HNO<sub>3</sub> by way of fluoride transfer (Huey et al., 1996;  
113 Amelynck et al., 2000; Crouse et al., 2006). Both methods are configured to allow for ion  
114 chemistry in a heated Teflon-coated flow tube at low pressure to selectively cluster the reagent  
115 ions with HNO<sub>3</sub> (HCl) in ambient air (Huey et al., 2004). The ions from the flow tube enter a mass  
116 spectrometer, where they are mass-analyzed and quantified. Gas-phase concentrations were  
117 reported in ppbv (parts-per-billion, by volume), and were subsequently converted to  $\mu\text{g m}^{-3}$  at  
118 ambient conditions prior to thermodynamic analysis. The estimated CIMS measurement  
119 uncertainty is 40%.



120

121 *Non-volatile aerosol cations and meteorological variables*

122 Non-volatile cations, such as  $\text{Na}^+$ ,  $\text{K}^+$ ,  $\text{Ca}^{2+}$ , and  $\text{Mg}^{2+}$ , were measured using the soluble acidic  
123 gases and aerosols (SAGA) instrumentation. Bulk aerosol (nominally  $< 4.1 \mu\text{m}$  aerodynamic  
124 diameter) are collected onto filters to quantify soluble ions (Dibb et al., 2003). Detection limits are  
125 5 pptv for  $\text{Mg}^{2+}$  and better than 20 pptv for  $\text{Na}^+$ ,  $\text{K}^+$ , and  $\text{Ca}^{2+}$   
126 ([https://cloud1.arc.nasa.gov/docs/intex-b/SAGA\\_Dibb.pdf](https://cloud1.arc.nasa.gov/docs/intex-b/SAGA_Dibb.pdf)). Filter sampling times were  
127 approximately 5 min or less. Units of NVCs were reported in  $\mu\text{g m}^{-3}$  under ambient conditions  
128 when used for thermodynamic calculations. Water vapor content was measured using a diode laser  
129 hygrometer (Diskin et al., 2002) and then converted to relative humidity based on the measurement  
130 of temperature measured onboard.

131

## 132 **2.2 Thermodynamic analysis of observations and PM sensitivity to aerosol precursors**

133 ISORROPIA II (Fountoukis and Nenes, 2007; <http://isorro피아.epfl.ch>), was used to calculate the  
134 equilibrium phase state and composition of inorganic aerosol systems containing  $\text{NH}_4^+$ ,  $\text{SO}_4^{2-}$ ,  
135  $\text{NO}_3^-$ ,  $\text{Cl}^-$ ,  $\text{Na}^+$ ,  $\text{Ca}^{2+}$ ,  $\text{K}^+$ ,  $\text{Mg}^{2+}$ , aerosol liquid water content, and partitioning of semi-volatile  
136 species (e.g. particle nitrate,  $\text{NO}_3^-$ , and gas phase nitric acid,  $\text{HNO}_3$ ). ISORROPIA was run in  
137 forward mode, which results in more robust and accurate predictions of pH owing to the sensitivity  
138 of reverse mode calculations to measurement uncertainty (Hennigan et al., 2015; Song et al., 2018).  
139 The model assumes that fine particles and their corresponding volatile counterparts are in  
140 thermodynamic equilibrium, which is a good assumption for submicron particles that are not  
141 kinetically limited by size (i.e., in the fine mode) (Dassios and Pandis 1999; Cruz and Pandis 2000;  
142 Fountoukis et al., 2009) and slow diffusivity in the particle phase. For the selected KORUS-AQ





143 dataset (<1 km ASL, 45% < RH < 95%, average RH: 62±12%; average temperature: 20.2±2.5 C)  
144 the aerosol tends to be in a liquid metastable state (i.e. no precipitation of salts under supersaturated  
145 conditions; Fountoukis and Nenes 2007; Day and Malm 2001; Seinfeld and Pandis, 2016).  
146 Efflorescence typically occurs for RH between 10-30%, however, such humidity points were not  
147 considered in our analysis.

148 While ISORROPIA II can handle systems containing non-volatile cations (NVCs), such as Na<sup>+</sup>,  
149 K<sup>+</sup>, Mg<sup>2+</sup>, and Ca<sup>2+</sup>, they were not considered in the analysis owing to their very low concentration  
150 (Figure 1) and minor impact on aerosol pH (Guo et al., 2018a); as well as, the fact that much of  
151 the NVCs were in the supermicron mode (Saide et al., 2019; Heim et al., 2020). A sensitivity  
152 calculation, using SAGA measurements as an upper limit of submicron NVCs pH confirms this  
153 (Table 1).

154 ISORROPIA II is used to calculate the pH of aerosols. pH is defined as:

$$155 \quad pH = -\log_{10}(\gamma_{H^+} H_{aq}^+) = -\log_{10}\left(\frac{1000 \gamma_{H^+} H_{air}^+}{W_i + W_o}\right) \approx -\log_{10}\left(\frac{1000 \gamma_{H^+} H_{air}^+}{W_i}\right) \quad (1)$$

156 where  $\gamma_{H^+}$  is the hydronium ion activity coefficient – here assumed to be unity,  $H_{aq}^+$  (mol L<sup>-1</sup>)  
157 hydronium ion concentration in aerosol liquid water,  $H_{air}^+$  (μg m<sup>-3</sup>) hydronium ion concentration  
158 per volume of air, and  $W_i$  (μg m<sup>-3</sup>) and  $W_o$  (μg m<sup>-3</sup>) are the particle liquid water concentrations  
159 associated with inorganic and organic species, respectively. Although  $W_o$  can be estimated, e.g.,  
160 through the hygroscopicity parameter (e.g., Guo et al., 2015), its effect on pH, together with  
161 organic effects on the activity coefficient, are secondary - introducing somewhere between a 0.15  
162 and 0.30 pH units change (Guo et al., 2015; Song et al., 2018; Vasilakos et al., 2018; Battaglia Jr.  
163 et al., 2019). Note Equation 1 is consistent with the “pH<sub>F</sub>” definition of Pye et al. (2020).



164 As applied here, the thermodynamic analysis provides pH consistent with “bulk” pH, which  
165 assumes that particles are internally mixed. This assumption tends to provide good estimates of  
166 pH for submicron particles, given that the equilibrium assumption is largely satisfied and semi-  
167 volatile partitioning of gases such as  $\text{NH}_3$  and  $\text{HNO}_3$  is well captured (Guo et al., 2018b, Pye et  
168 al., 2020). Internal mixing is achieved in a few hours in polluted areas due to rapid secondary  
169 aerosol production (Wang et al., 2010; Zhu et al., 2016; Riemer et al., 2019). Both the ground  
170 AMS (Kim et al., 2018) and the aircraft AMS (Nault et al., 2018) saw no evidence of external  
171 mixing based on the mass size distributions of the individual components, so the internal mixing  
172 assumption is appropriate.

173 The results of the thermodynamic analysis are then combined with the conceptual framework of  
174 Nenes et al. (2020a) to identify the chemical domains of PM mass sensitivity to  $\text{HNO}_3$  and  $\text{NH}_3$   
175 availability for this observational dataset. These sensitivity domains are characterized as *i*)  
176 primarily  $\text{NH}_3$ -sensitive, *ii*) primarily  $\text{HNO}_3$ -sensitive, *iii*) combined  $\text{NH}_3$  and  $\text{HNO}_3$  sensitive,  
177 and, *iv*)  $\text{HNO}_3$ /  $\text{NH}_3$  insensitive. This thermodynamically consistent approach enables us to  
178 directly determine how change in gas phase species will elicit a change in PM mass. As it pertains  
179 to the KORUS-AQ campaign, we adopt the Nenes et al. (2020a) threshold value for nitrate and  
180 ammonia partitioning that separates each regime at the 10% level. For example, for nitrate this  
181 means that when more than 10% of the total nitrate is in the particle phase, we would expect PM  
182 responses to  $\text{NO}_3^-$  precursors to be significant.

183

#### 184 **2.4 Nitrate partitioning constrained pH (NPC-pH)**

185 When the thermodynamic model is run in forward mode, input of semi-volatile species (i.e., those  
186 that can exist in particle- or gas-phase) are assumed to be total gas and particle concentrations. As



187 in this study, when  $\text{NH}_3$  data is unavailable, the total  $\text{NH}_3$  will be lower than the true value, as  
188 some fraction of the total  $\text{NH}_3$  is actually in the gas phase. In these cases, particle acidity is likely  
189 to be overestimated. Past studies have proposed an iterative approach to calculate pH and gas phase  
190 ammonia data (e.g., Guo et al., 2016) that involves running ISORROPIA (without gas-phase  
191 ammonia) to retrieve the predicted equilibrium gas phase ammonia concentration from the model  
192 output. This equilibrium  $\text{NH}_3$  along with the measured  $\text{NH}_4^+$  is then used as total ammonia input  
193 for the next ISORROPIA iteration (which eventually adds some mass to the system), holding all  
194 other input values constant. After each such iteration, convergence is checked by examining  
195 whether the values of gas-phase  $\text{NH}_3$  agree to within a predefined criterion. This method, however,  
196 is unconditionally unstable, i.e., the method does not converge when an increasingly strict criterion  
197 is used (see Figure 2 for a schematic). To demonstrate this, Figure 3 presents how pH and gas-  
198 phase  $\text{NH}_3$  change with iteration; a stable algorithm would eventually converge to values that do  
199 not change with iteration; in reality  $\text{NH}_3$  and pH increase monotonically without a bound. This  
200 instability is not unique to ISORROPIA, but inherent to the algorithm and should apply to any  
201 thermodynamic model, as the amount of total ammonia with every iteration increases – without  
202 any bound. Applying a less strict upper bound would result in an arbitrary estimate of total  
203 ammonia, which requires some prior knowledge on  $\text{NH}_3$  levels to provide realistic values of pH  
204 (which is what Guo et al., 2016 adopted).

205 As an alternative to the Guo et al. (2016) algorithm, we propose a method to infer pH calculations  
206 from thermodynamic analysis of observations when  $\text{NH}_3$  data are lacking. This approach involves  
207 using an algorithm that is tied to the observed nitrate/nitric acid partitioning (hereafter referred to  
208 as “nitrate partitioning constrained pH”, NPC-pH) to infer gas-phase  $\text{NH}_3$  concentrations required  
209 for plausible pH predictions. Figure 4 summarizes the methodology behind this approach. The



210 observed  $\text{NH}_4^+$ , total nitrate, and nitrate partitioning fraction,  $\epsilon(\text{NO}_3)$ —defined as the fraction of  
211 total nitrate (gas + aerosol) present in the aerosol phase—are used as input to an iterative algorithm  
212 that determines the value of gas-phase  $\text{NH}_3$  that, together with the observed value of  $\text{NH}_4^+$ ,  
213 temperature, and relative humidity reproduces the observed  $\epsilon(\text{NO}_3)$  to some predetermined level  
214 of accuracy. The thermodynamic calculations required for each step in the iterative procedure are  
215 done with ISORROPIA-II. Upon convergence (here, to within  $10^{-6}$  between iterations), particle  
216 liquid water,  $\text{H}^+$ <sub>air</sub> concentration, and particle pH are obtained and used for further analysis. In the  
217 following, we assess the predicted pH with NPC-pH, which together with aerosol liquid water  
218 content is needed to determine an effective PM control strategy.

219 Nitric acid can condense onto fine mode and coarse particles containing non-volatile cations (from  
220 seasalt or dust). Because of this, nitrate may over time volatilize and recondense onto coarse mode  
221 cations forming nonvolatile species (in the form of  $\text{Ca}(\text{NO}_3)_2$ ,  $\text{NaNO}_3$  and other salts). This  
222 disequilibrium will lead to a gas phase  $\text{HNO}_3$  concentration which is lower than the equilibrium  
223 value expected from the  $\text{PM}_{10}$  composition and higher than the corresponding value based on the  
224 coarse mode composition. Given that the equilibration timescale of submicron aerosol is much  
225 smaller than for coarse mode particles, the degree of disequilibrium between the  $\text{PM}_{10}$  nitrate and  
226 gas-phase  $\text{HNO}_3$  is much smaller than that for coarse mode nitrate. We therefore assume that the  
227  $\text{PM}_{10}$  semi-volatile inorganic species ( $\text{NO}_3^-$ ,  $\text{NH}_4^+$ ) are in equilibrium with their gas phase  
228 components ( $\text{HNO}_3$ ,  $\text{NH}_3$ ). Analysis carried out by Guo et al. (2017) supports this approach.

229

## 230 **2.5 Data selection and analysis**

231 Data points were filtered for conditions where ambient relative humidity (RH) fell within the range  
232 of 45-95%, and flight altitude below 1 km which is often within the boundary layer and most



233 relevant from an air quality perspective (the sampling RH was often significantly lower, but  
234 exposure to these low levels of humidity is too short to have a significant impact on semi-volatile  
235 nitrate and ammonium; Shingler et al, 2016; Guo et al., 2017). The RH range was chosen to ensure  
236 robust estimations from the thermodynamic model. Data for  $RH > 95\%$  were excluded owing to  
237 the exponential growth in particle liquid water with RH, which leads to high  $W_i$  and subsequently  
238 large pH uncertainty owing to propagation of RH uncertainties (Guo et al., 2015). Guo et al. (2016)  
239 suggests that below RH of 40%, pH estimations are subject to considerable uncertainty owing to  
240 the low aerosol liquid water and other uncertainties, which limits the ability to capture the observed  
241 partitioning of nitrate and other species. From this filtering process, a total of 11 of the total flights  
242 were analyzed and are summarized in Table S1.

243

### 244 **3. Results**

#### 245 **3.1 Sensitivity studies to evaluate the new NPC-pH algorithm**

246 The NPC-pH algorithm for predicting pH without  $NH_3$  data was assessed based on a synthetic  
247 dataset for which aerosol is in perfect thermodynamic equilibrium. To this dataset, random  
248 variability is added to the concentration of semi-volatile species (within a predefined but relatively  
249 wide range). The NPC-pH algorithm was applied to the original and noisy synthetic data sets, to  
250 predict pH. The aerosol acidity obtained from NPC-pH was then compared to the pH of the initial  
251 data where the aerosol was in equilibrium with all species. The robustness of the acidity to noise  
252 level is important, especially given that aerosol semivolatile species could be in disequilibrium.

253 The synthetic data was constructed of aerosol precursor values relevant for KORUS-AQ  
254 conditions: total  $NO_3$  concentration ranged from 0.2 to  $110 \mu g m^{-3}$  allowing for  $\epsilon(NO_3)$  to range



255 from 0-0.95. Total  $\text{SO}_4$  and total  $\text{NH}_4^+$  concentrations ranged from  $0.1\text{-}10\ \mu\text{g m}^{-3}$  and  $0.2\text{-}110\ \mu\text{g}$   
256  $\text{m}^{-3}$ , respectively.  $\epsilon(\text{NH}_4)$  ranged from 0-1. The total Cl concentration was kept constant at  $0.50$   
257  $\mu\text{g m}^{-3}$  and NVC concentrations were set to zero. Temperature was kept constant at 298K, and the  
258 RH ranged from 45-95%. Comparing the equilibrium partitioning retrieved from the synthetic data  
259 (without added noise) to that generated from the algorithm resulted in nearly perfect agreement  
260 between the two quantities, when  $\epsilon(\text{NO}_3)$  was greater than about 40% (Figure 5). Higher sensitivity  
261 of low  $\epsilon(\text{NO}_3)$  values to pH and gas-phase  $\text{NH}_3$  results in more scatter in  $\epsilon(\text{NO}_3)$  generated from  
262 the algorithm for  $\epsilon(\text{NO}_3) < 0.4$ . Average pH for the whole synthetic dataset for equilibrium and  
263 NPC-pH method are  $2.14 \pm 1.33$  and  $2.26 \pm 1.25$ , respectively while the average LWC for  
264 equilibrium and NPC-pH method are  $42.50 \pm 137.85\ \mu\text{g m}^{-3}$  and  $42.25 \pm 137.93\ \mu\text{g m}^{-3}$ ,  
265 respectively. The large standard deviation is a result of a wide range of conditions tested during  
266 the analysis.

267 To ascertain how uncertainties in nitrate partitioning (i.e., deviations from thermodynamic  
268 equilibrium) would impact pH inferences from NPC-pH, random noise at the 1-50% level is added  
269 to the original  $\epsilon(\text{NO}_3)$  values from the synthetic dataset. Reapplication of NPC-pH to the noisy  
270 datasets then quantify the effect of this noise to the inferred pH. The method used to add noise is  
271 shown in equations 2 and 3

$$272 \quad X = 2\Phi\left(-\frac{1}{2} + Rnd\right)\epsilon(\text{NO}_3) \quad (2)$$

$$273 \quad \epsilon(\text{NO}_3)_{Rnd} = \epsilon(\text{NO}_3) + X \quad (3)$$

274 where  $\epsilon(\text{NO}_3)_{Rnd}$  is  $\epsilon(\text{NO}_3)$  with added random noise X that is symmetrical about zero and scaled  
275 to the magnitude of  $\epsilon(\text{NO}_3)$ ;  $\Phi$  is the maximum fractional noise level (ranging from 0.01-0.5 to  
276 express a noise level of 1-50%) and  $Rnd$  is a random number between 0 and 1, generated by the  
277 "rand()" pseudorandom number generator available in the Matlab® environment.



278 Results from this sensitivity analysis reveal that a 50% relative error in  $\varepsilon(\text{NO}_3)$  resulted in an  
279 average absolute error in pH of  $0.28 \pm 0.45$  units, and explained as follows. Figure 6 presents  
280  $\varepsilon(\text{NO}_3)$ ,  $\varepsilon(\text{NH}_4)$  and pH for  $T = 288$  K, and with average ISORROPIA-predicted liquid water  
281 content ( $13.78 \pm 10.52 \mu\text{g m}^{-3}$ ) and activity coefficients (0.125 and 1.794 for  $\gamma_{\text{NO}_3} - \gamma_{\text{H}^+}$  and  
282  $\gamma_{\text{H}^+} / \gamma_{\text{NH}_4^+}$ , respectively) derived from the KORUS-AQ flight data analysis (Table 1). In the blue  
283 region, where  $\varepsilon(\text{NO}_3)$  approaches 0 or 1, we observe that a small uncertainty in  $\varepsilon(\text{NO}_3)$  can result  
284 in significant changes to pH. In the pink region, however, we would expect that even large changes  
285 in  $\varepsilon(\text{NO}_3)$  would only result in minor changes to pH. Evaluating  $0.2 < \varepsilon(\text{NO}_3) < 0.8$  from the  
286 synthetic data resulted in an average absolute error in pH of  $0.21 \pm 0.15$  units. Therefore, pH  
287 predictions using this method are reasonably accurate, especially when considering the inherent  
288 uncertainty of pH inferences using thermodynamic models (Pye et al. 2020) and the low sensitivity  
289 of pH to  $\text{NH}_3$  inferences error (about a factor of 10 error in  $\text{NH}_3$  provides a pH error of 1 unit,  
290 regardless of acidity regime; Guo et al., 2017; Song et al., 2019).

291

### 292 **3.2 Aerosol acidity during KORUS-AQ**

293 KORUS-AQ integrated aircraft and ground-based measurements, and satellite observations. The  
294 campaign was conducted over South Korea (33 and 39 °N, 124 and 130E °E) and the Yellow Sea  
295 during the months of May and June in 2016. Flight tracks for the DC-8 during KORUS-AQ are  
296 shown in Figure 7, colored by measured concentrations of  $\text{NO}_3^-$ . Most flights focused on the  
297 western region (35 and 38 °N, 126 and 127°E) of South Korea extending into the Yellow Sea.  
298 Major emitters of  $\text{NO}_x$  are the Taean coal power plant (36.90 °N, 126.23 °E), Dangjin power plant  
299 (37.06°N, 126.51°E), and Yeongheung power station (37.24°N, 126.44°E) – which are all within  
300 the region of observed high nitrate concentrations (Hong et al. 2019; Kafle et al. 2017; Kim et al.



301 2013). Increased nitrate levels observed in Table 1 for Asia are most likely the result of emissions  
302 from vehicular traffic and power plants, and active photochemistry (Nault et al., 2018) and  
303 nighttime nitrate formation from  $\text{N}_2\text{O}_5$  hydrolysis (Jordan et al., 2019). More details on KORUS-  
304 AQ flights can be found in Nault et al. (2018).

305 Measurements of  $\text{HNO}_3$  and  $\text{NO}_3^-$  indicate that  $\epsilon(\text{NO}_3)$  most of the time (approximately 92%;  
306 Figure S3) falls between 0.1 and 0.9, indicating that aerosol nitrate levels will be sensitive to pH  
307 (i.e., reside in the “sensitivity window” of Vasilakos et al., 2018; Figure 6). Of the remaining 8%,  
308 approximately 6% of these partitioning values fall below 0.1, while 2% of all nitrate partitioning  
309 measurements were greater than 0.9, where nitrate partitioning is expected to be less sensitive to  
310 pH changes. Given this and the sensitivity analysis of Section 3.1, the NPC-pH algorithm can  
311 provide robust estimates of aerosol pH for the majority of the KORUS-AQ data. We find that the  
312 average pH for all flights was  $2.43 \pm 0.68$  (Table 1), while the average acidity between flights varied  
313 between 1.74 and 2.90 (Table S1). These pH levels are similar to what has been reported by others  
314 in the region for summertime conditions; Spring in Beijing, China (pH range= 1.8-4.3) (Ding et  
315 al., 2019; Tan et al., 2018; Wang et al., 2019; Pye et al. 2020).

316 The inorganic fraction of the KORUS-AQ aerosol is dominated by sulfate, ammonium, and nitrate  
317 (Figure 1). Since as already mentioned in the methods the relative mass concentrations of NVCs  
318 to other major inorganic ion components are low, we assume the formation of nonvolatile salts  
319 (e.g.  $\text{Ca}(\text{NO}_3)_2$  and  $\text{Na}(\text{NO}_3)$ ) negligibly impact the pH derived from nitrate partitioning. This  
320 assumption is valid as the pH calculated using SAGA measurements of NVCs is within 1% of that  
321 predicted, consistent with the impact suggested by Guo et al. (2018a). We also do not consider the  
322 contribution of organic nitrates to the total amount of nitrates (which constitute less than 10% of





323 the total nitrate, hence have a minimal impact on liquid water content and pH, based on the analysis  
324 in Section 3.1).

325 Particle pH is affected by several coupled variables such as particle nitrate and nitrate partitioning  
326 levels. Higher ambient particle pH is often associated with higher concentrations of particle nitrate  
327 (Guo et al., 2018b). This occurs when nitrate aerosol (usually in the form of ammonium nitrate)  
328 dominates the aerosol liquid water content; in such situations, the aerosol can contain considerable  
329 amounts of aerosol water but maintain small amounts of  $H^+$  in solution – as it tends to combine  
330 with  $NO_3^-$  to form volatile  $HNO_3$ . In contrast, when aerosol liquid water is controlled by  
331 hygroscopic sulfates, significant amounts of  $H^+$  can exist in solution (e.g., from the semi-volatile  
332 partitioning of  $NH_4^+$  to form  $NH_3$ ) as its tendency to associate with  $HSO_4^-$ ,  $SO_4^{2-}$  is relatively weak  
333 and sulfates are involatile. This general effect of higher (lower) pH associated with higher (lower)  
334  $NO_3$  has been seen in a number of other field campaigns (see comparisons in Table 1). In Cabauw,  
335 Netherlands during the summer, Guo et al. (2018b) reported an  $\epsilon(NO_3)$  of 88%, with a  
336 corresponding pH of  $3.3 \pm 0.5$ . Both quantities are higher than the values found for the KORUS-  
337 AQ campaign. The pH of aerosol in Beijing, China in the summer was found to be  $3.9 \pm 1.3$  for  
338 nitrate levels that are higher than those measured for the South Korean data (Table 1).

339

### 340 **3.3 Acidity and PM sensitivity regimes to $NH_3$ and $HNO_3$ during KORUS-AQ**

341 Nenes et al. (2020a) developed a framework that allows PM sensitivity to  $NH_3$  and  $HNO_3$   
342 availability to be determined from aerosol acidity and liquid water content. This framework  
343 directly determines effective PM reduction policies – which is important given recent work  
344 identifying  $NH_3$  reductions over other policies (e.g.,  $NO_x$  and  $SO_x$  reductions) (Pozzer et al., 2017;



345 Xu et al., 2019) as the most effective for PM reductions, and the dominance of PM in the region  
346 by ammonium and nitrate (22.2 and 36.6%, respectively; Figure 1)

347 In its simplest form, the Nenes et al. (2020a) framework is expressed in terms of a “policy map”  
348 (Figure 8) characterized by four distinct regimes: one, shaded pink, where  $\epsilon(\text{NO}_3)$  is small and  
349  $\epsilon(\text{NH}_4)$  is large (i.e., the majority of nitrate resides in the gaseous phase and ammonia in the particle  
350 phase, defined by a relevant threshold); here PM mass responds proportionally to changes in the  
351 total ammonia but tends to be insensitive to total nitrate changes. For this reason, Nenes et al.  
352 (2020a) characterize PM in this regime as being “NH<sub>3</sub> sensitive”. The opposite is seen in the blue-  
353 shaded regime, as the majority of nitrate resides in the aerosol phase and ammonia in the gas phase.  
354 For this reason, Nenes et al. (2020a) characterize PM in this region as being “HNO<sub>3</sub> sensitive”. In  
355 both acidity regimes, partitioning may not be strongly affected by pH changes, therefore  
356 uncertainties in its exact value carry minor implications for PM sensitivity to available ammonia  
357 and nitrate. In the purple acidity domain, however, which Vasilakos et al. (2018) terms “sensitivity  
358 window”, PM tends to respond to both HNO<sub>3</sub> and NH<sub>3</sub> emissions, as an important fraction of both  
359 species is in the aerosol phase (Nenes et al., 2020a). Here, rather precise knowledge of aerosol pH  
360 is important – as variations to within one unit usually imply a very large change in the partitioning  
361 fraction for each semi-volatile species, hence PM sensitivity. The fourth domain, colored white, is  
362 characterized by low nitrate and ammonium partitioning fraction, and PM is then relatively  
363 insensitive to changes in NH<sub>3</sub> and HNO<sub>3</sub> availability.

364 From the histogram of observed nitrate partitioning (Figure S3), we expect a large fraction of the  
365 data to lie in the HNO<sub>3</sub>/NH<sub>3</sub> sensitive domain. As distribution of nitrate partitioning is toward the  
366 high end of  $\epsilon(\text{NO}_3)$  for the study (average nitrate partitioning value of  $58 \pm 24\%$ ), PM<sub>1</sub> reductions  
367 would be sensitive to reductions in HNO<sub>3</sub> – hence NO<sub>x</sub> reductions. Indeed, if the pH and aerosol



368 liquid water content for the KORUS-AQ data are plotted on the policy map (Figure 8), the data  
369 reside in the domain where  $\text{HNO}_3$  or a mix of  $\text{HNO}_3/\text{NH}_3$  controls are generally the most effective  
370 routes for reduction of inorganic  $\text{PM}_{10}$  mass for the time period of the study.

371 Focusing on flights that span the nitrate  $\epsilon(\text{NO}_3)$  range with high  $\text{HNO}_3$  availability provides  
372 additional insights on effective PM controls: during flight 19 the highest levels of nitrate and  
373 ammonium of the mission were measured; and in contrast during flight 15 approximately 30% of  
374 its ambient nitrate partitioning values fell below 0.1 (Figure S4; other per-flight characteristics can  
375 be found in table S1). High levels of nitrate availability are expected for flight 19 because of its  
376 proximity to a number of power plants (and associated  $\text{NO}_x$  emissions) along the northwest coast.  
377 The DC-8 aircraft also flew very close to Seoul, South Korea for this flight (see Figure S1) – an  
378 area where nitrate availability from vehicular  $\text{NO}_x$  emissions are expected to be large. Plotting the  
379 data from both flights on the Nenes et al. (2020a) policy map indicates where the high  $\text{HNO}_3$   
380 availability can lead to high  $\text{NO}_3^-$  levels. The results (Figure 9) suggest that data from each flight  
381 reside mostly in the  $\text{NH}_3$ - $\text{HNO}_3$  sensitivity domain, which implies similar emissions control  
382 strategies are effective, despite the very different aerosol characteristics in both flights.

383 The above analysis can be further expanded to consider only PM levels above a regulatory mass  
384 threshold, as PM control policies are most effective when relevant for the high PM levels seen in  
385 pollution events. To assess this, we plot all the available data on the policy map, but with points  
386 color-coded with PM level (Figure 10). For PM levels exceeding e.g.,  $30 \mu\text{g m}^{-3}$ ,  $\text{HNO}_3$  is always  
387 an effective control strategy, while  $\text{NH}_3$  is effective for about half the points. The relatively fewer  
388 cases that fall into the  $\text{NH}_3$ -sensitive domain are characterized by low PM levels, hence less  
389 important to control. Given that dry deposition dominates the loss of boundary layer PM during  
390 haze episodes, and the expected low deposition rate of nitrate when  $\epsilon(\text{NO}_3)$  is relatively large



391 (Nenes et al., 2020b) further emphasizes the need to control  $\text{NO}_x$ , as such conditions favor the  
392 rapid accumulation of available  $\text{HNO}_3$  – and buildup of the high levels of  $\text{NO}_3^-$  seen in the  
393 observations (Figure 1).

#### 394 **4. Summary and broader implications**

395 Accurate estimates of atmospheric aerosol acidity are important for understanding a number of  
396 atmospheric processes sensitive to pH. Here, we present a method – called NPC-pH - for  
397 estimating aerosol pH, through thermodynamic analysis of observations that lack gas-phase  
398 ammonia measurements. NPC-pH is based on the observed gas-to-particle partitioning of nitrate  
399 in the absence of ammonia measurements, and is shown to perform much better than a previously  
400 proposed algorithm that iterated for total ammonia (using aerosol ammonium as an initial guess),  
401 as the latter is shown to be unconditionally unstable. NPC-pH is also shown to provide robust pH  
402 levels that are relatively insensitive to nitrate partitioning errors.

403 Applying NPC-pH to airborne observations collected from the NASA/NIER KORUS-AQ field  
404 campaign in South Korea resulted in pH predictions ( $\text{pH}=2.43 \pm 0.68$ ) that are consistent with  
405 published estimates in this region and season. The pH and LWC calculated from our  
406 thermodynamic analysis and the approaches of Nenes et al. (2020ab) determine the “chemical  
407 regime” of PM sensitivity to ammonia and nitrate availability, and, “dry deposition velocity  
408 regime” of inorganic nitrogen (which controls the lifetime, hence accumulation, of nitrate in the  
409 boundary layer during haze episodes). For KORUS-AQ, we found that the aerosol formation is  
410 often in the  $\text{NH}_3$  and  $\text{HNO}_3$ -sensitive or  $\text{HNO}_3$ -sensitive zone, while a small fraction (4%) of the  
411 points fall in  $\text{NH}_3$ -limited region near the Yellow Sea, Jeju Island, Busan and Eastern Sea.  
412 Nevertheless, when PM levels are high, the data always lies in the  $\text{HNO}$ -sensitive or  $\text{HNO}_3/\text{NH}_3$   
413 – sensitive region. Under these conditions, we conclude that  $\text{HNO}_3$  reductions prove to be the most



414 effective for all conditions examined, and that  $\text{NH}_3$  emissions would only partially be effective in  
415 reducing PM levels – especially given that during pollution episodes, the pH and LWC levels  
416 promote rapid accumulation of nitrate aerosol in the boundary layer owing to its slow dry  
417 deposition (Nenes et al., 2020b). A complete in-depth analysis of the complex chemistry and  
418 contributions of different sources however is required to fully assess the most effective  $\text{NO}_x$   
419 emission controls to reduce  $\text{HNO}_3$  production. Source attribution information can also be  
420 represented on the policy maps shown here to understand their role in shaping the acidity, liquid  
421 water, and PM sensitivity/deposition regimes (e.g., Zang et al., in review) to further refine types  
422 of policies that could be effective during pollution episodes.

423 Despite the benefits of controlling PM formation to reduce ammonium-nitrate aerosol and PM  
424 mass, we must consider that the acidity domain can significantly affect other processes and sources  
425 of aerosol toxicity. Fang et al. (2017) and Wong et al. (2020) showed that acid-driven dissolution  
426 of transition metals (e.g., Fe, Cu) can potentiate health effects such as cardiovascular morbidity  
427 and mortality through oxidative stress (Bates et al., 2015; Ghio et al., 2012). If emissions controls,  
428 in an attempt to reduce PM levels also lead to reduction in pH, may unintentionally increase aerosol  
429 toxicity with adverse health effects in humans. Lastly, increased aerosol acidity can impact the  
430 deposition pattern of reactive nitrogen (Nenes et al., 2020b) and bioavailability of micronutrients  
431 (e.g. Fe, P) with both synergistic and/or antagonistic effects on remote ecosystems (e.g.,  
432 Meskhidze et al., 2003; Nenes et al., 2011; Ito et al., 2016).

433

#### 434 **Acknowledgements**

435 This work was supported by NASA grant NNX16AE19G (KORUS-AQ) and from PyroTRACH  
436 (ERC-2016-COG) funded from H2020-EU.1.1. - Excellent Science - European Research Council



437 (ERC), project ID 726165. JLJ, PCJ, and BAN (AMS) were supported by NASA grants  
438 NNX15AT96G, 80NSSC19K0124, and 80NSSC18K0630. JDC, MKJ, AT, and POW (Caltech)  
439 were supported by NASA grants NNX15AT97G.

440

#### 441 **Author contributions**

442 II was responsible for the thermodynamic analysis of the ambient data, contributed to the ammonia  
443 estimation algorithm and wrote the initial draft of the manuscript with significant contributions by  
444 AN and RW. AN is a core developer of ISORROPIA-II, developed the conceptual framework used  
445 here for understanding the sensitivity of PM<sub>2.5</sub> to total nitrate and ammonia, the tools to include  
446 the ambient data on the acidity maps and also demonstrated the unconditional instability of the  
447 original NH<sub>3</sub> iteration algorithm of Guo et al. (2016). AN and RW were involved in planning and  
448 supervision of the work. All authors provided feedback on the analysis approach and extensively  
449 contributed to the manuscript text.

450

#### 451 **Code and Data availability**

452 The ISORROPIA-II thermodynamic equilibrium code is available at <http://isorropia.epfl.ch>.  
453 KORUS-AQ data is available at <https://www-air.larc.nasa.gov/cgi-bin/ArcView/korusaq>.

454

#### 455 **Competing interests**

456 The authors declare that they have no conflicts of interest.



## 457 **References**

- 458 Amelynck, C., N. Schoon, and E. Arijs. Gas phase reactions of CF<sub>3</sub>O<sup>-</sup> and CF<sub>3</sub>O-H<sub>2</sub>O with  
459 nitric, formic, and acetic acid, *International Journal of Mass Spectrometry*, 203: 165-75, 2000
- 460 Bahreini, R., B. Ervens, A. M. Middlebrook, C. Warneke, J. A. de Gouw, P. F. DeCarlo, J. L.  
461 Jimenez, C. A. Brock, J. A. Neuman, T. B. Ryerson, H. Stark, E. Atlas, J. Brioude, A. Fried, J. S.  
462 Holloway, J. Peischl, D. Richter, J. Walega, P. Weibring, A. G. Wollny, and F. C. Fehsenfeld.  
463 Organic aerosol formation in urban and industrial plumes near Houston and Dallas, Texas, *Journal*  
464 *of Geophysical Research: Atmospheres*, 114, 2009
- 465 Bates, Josephine T., Rodney J. Weber, Joseph Abrams, Vishal Verma, Ting Fang, Mitchel Klein,  
466 Matthew J. Strickland, Stefanie Ebel Sarnat, Howard H. Chang, James A. Mulholland, Paige E.  
467 Tolbert, and Armistead G. Russell. Reactive Oxygen Species Generation Linked to Sources of  
468 Atmospheric Particulate Matter and Cardiorespiratory Effects, *Environmental Science &*  
469 *Technology*, 49: 13605-12, 2015
- 470 Chen, Y., Xu, L., Humphry, T., Hettiyadura, A. P. S. S., Ovadnevaite, J., Huang, S., Poulain, L.,  
471 Schroder, J. C., Campuzano-Jost, P., Jimenez, J. L., Herrmann, H., O'Dowd, C., Stone, E. A., Ng,  
472 N. L., O'Dowd, C., Stone, E. A., Ng, N. L., O'Dowd, C., Stone, E. A. and Ng, N. L.: Response of  
473 the Aerodyne Aerosol Mass Spectrometer to Inorganic Sulfates and Organosulfur Compounds:  
474 Applications in Field and Laboratory Measurements, *Environ. Sci. Technol.*, 53(9), 5176–5186,  
475 doi:10.1021/acs.est.9b00884, 2019
- 476 Crouse, John D., Karena A. McKinney, Alan J. Kwan, and Paul O. Wennberg. Measurement of  
477 Gas-Phase Hydroperoxides by Chemical Ionization Mass Spectrometry, *Analytical Chemistry*, 78:  
478 6726-32, 2006
- 479 Cruz, Celia N., and Spyros N. Pandis. Deliquescence and Hygroscopic Growth of Mixed  
480 Inorganic–Organic Atmospheric Aerosol, *Environmental Science & Technology*, 34: 4313-19,  
481 2000
- 482 Dassios, Konstandinos G., and Spyros N. Pandis. The mass accommodation coefficient of  
483 ammonium nitrate aerosol, *Atmospheric Environment*, 33: 2993-3003, 1999



- 484 Dawson, M. L., V. Perraud, A. Gomez, K. D. Arquero, M. J. Ezell, and B. J. Finlayson-Pitts.  
485 Measurement of gas-phase ammonia and amines in air by collection onto an ion exchange resin  
486 and analysis by ion chromatography, *Atmos. Meas. Tech.*, 7: 2733-44, 2014
- 487 Day, Derek, and William Malm. Aerosol light scattering measurements as a function of relative  
488 humidity: A comparison between measurements made at three different sites, *Atmospheric*  
489 *Environment*, 35: 5169-76, 2001
- 490 DeCarlo, P. F., E. J. Dunlea, J. R. Kimmel, A. C. Aiken, D. Sueper, J. Crouse, P. O. Wennberg,  
491 L. Emmons, Y. Shinozuka, A. Clarke, J. Zhou, J. Tomlinson, D. R. Collins, D. Knapp, A. J.  
492 Weinheimer, D. D. Montzka, T. Campos, and J. L. Jimenez. Fast airborne aerosol size and  
493 chemistry measurements above Mexico City and Central Mexico during the MILAGRO campaign,  
494 *Atmos. Chem. Phys.*, 8: 4027-48, 2008
- 495 DeCarlo, Peter, Joel Kimmel, Achim Trimborn, Megan Northway, John Jayne, Allison Aiken,  
496 Marc Gonin, Katrin Fuhrer, Thomas Horvath, Kenneth Docherty, Doug Worsnop, and Jose  
497 Jimenez. Field-Deployable, High-Resolution, Time-of-Flight Aerosol Mass Spectrometer,  
498 *Analytical Chemistry*, 78: 8281-9, 2007
- 499 Dibb, J. E., Talbot, R. W., Scheuer, E. M., Seid, G., Avery, M. A., and Singh, H. B.: Aerosol  
500 chemical composition in Asian continental outflow during the TRACE-P campaign: Comparison  
501 with PEM-West B, *J. Geophys. Res.*, 108, 8815, <https://doi.org/10.1029/2002JD003111>, 2003
- 502 Ding, J., P. Zhao, J. Su, Q. Dong, X. Du, and Y. Zhang. Aerosol pH and its driving factors in  
503 Beijing, *Atmos. Chem. Phys.*, 19: 7939-54, 2019
- 504 Diskin, G. S., Podolske, J. R., Sachse, G. W. and Slate, T. A.: Open-path airborne tunable diode  
505 laser hygrometer, in *Diode Lasers and Applications in Atmospheric Sensing*, vol. 4817, pp. 196–  
506 204, International Society for Optics and Photonics., 2002
- 507 Drewnick, F., S. S. Hings, M. R. Alfarra, A. S. H. Prevot, and S. Borrmann. Aerosol quantification  
508 with the Aerodyne Aerosol Mass Spectrometer: detection limits and ionizer background effects,  
509 *Atmos. Meas. Tech.*, 2: 33-46, 2009
- 510 Dunlea, E. J., P. F. DeCarlo, A. C. Aiken, J. R. Kimmel, R. E. Peltier, R. J. Weber, J. Tomlinson,  
511 D. R. Collins, Y. Shinozuka, C. S. McNaughton, S. G. Howell, A. D. Clarke, L. K. Emmons, E.  
512 C. Apel, G. G. Pfister, A. van Donkelaar, R. V. Martin, D. B. Millet, C. L. Heald, and J. L. Jimenez.





- 513 Evolution of Asian aerosols during transpacific transport in INTEX-B, *Atmos. Chem. Phys.*, 9:  
514 7257-87, 2009
- 515 Duyzer, J. Dry deposition of ammonia and ammonium aerosols over heathland, *Journal of*  
516 *Geophysical Research: Atmospheres*, 99: 18757-63, 1994
- 517 Fang, T., Guo, H. Zeng, L., Verma, V., Nenes, A., and Weber, R.J. Highly Acidic Ambient  
518 Particles, Soluble Metals, and Oxidative Potential: A Link between Sulfate and Aerosol Toxicity,  
519 *Environmental Science & Technology*, 51: 2611-20, 2017
- 520 Farmer, D. K., A. Matsunaga, K. S. Docherty, J. D. Surratt, J. H. Seinfeld, P. J. Ziemann, and J.  
521 L. Jimenez. Response of an aerosol mass spectrometer to organonitrates and organosulfates and  
522 implications for atmospheric chemistry, *Proceedings of the National Academy of Sciences*, 107:  
523 6670-75, 2010
- 524 Fountoukis, C., and A. Nenes. ISORROPIA II: a computationally efficient thermodynamic  
525 equilibrium model for  $K^+$  -  $Ca^{2+}$  -  $Mg^{2+}$  -  $NH_4^+$  -  $Na^+$  -  $SO_4^{2-}$  -  $NO_3^-$  -  $Cl^-$  -  $H_2O$  aerosols,  
526 *Atmos. Chem. Phys.*, 7: 4639-59, 2007
- 527 Fountoukis, C., A. Nenes, A. Sullivan, R. Weber, T. Van Reken, M. Fischer, E. Matías, M. Moya,  
528 D. Farmer, and R. C. Cohen. Thermodynamic characterization of Mexico City aerosol during  
529 MILAGRO 2006, *Atmos. Chem. Phys.*, 9: 2141-56, 2009
- 530 Fry, J. L., Draper, D. C., Zarzana, K. J., Campuzano-Jost, P., Day, D. A., Jimenez, J. L., Brown,  
531 S. S., Cohen, R. C., Kaser, L., Hansel, A., Cappellin, L., Karl, T., Hodzic Roux, A., Turnipseed,  
532 A., Cantrell, C., Lefer, B. L. and Grossberg, N.: Observations of gas- and aerosol-phase organic  
533 nitrates at BEACHON-RoMBAS 2011, *Atmos. Chem. Phys.*, 13(17), 8585–8605,  
534 doi:10.5194/acp-13-8585-2013, 2013
- 535 Ghio, Andrew J., Martha Sue Carraway, and Michael C. Madden. Composition of Air Pollution  
536 Particles and Oxidative Stress in Cells, Tissues, and Living Systems, *Journal of Toxicology and*  
537 *Environmental Health, Part B*, 15: 1-21, 2012
- 538 Guo, H., J. Liu, K. D. Froyd, J. M. Roberts, P. R. Veres, P. L. Hayes, J. L. Jimenez, A. Nenes, and  
539 R. J. Weber. Fine particle pH and gas–particle phase partitioning of inorganic species in Pasadena,  
540 California, during the 2010 CalNex campaign, *Atmos. Chem. Phys.*, 17: 5703-19, 2017



- 541 Guo, H., A. Nenes, and R. J. Weber. The underappreciated role of nonvolatile cations in aerosol  
542 ammonium-sulfate molar ratios, *Atmos. Chem. Phys.*, 18: 17307-23, 2018a
- 543 Guo, H., R. Otjes, P. Schlag, A. Kiendler-Scharr, A. Nenes, and R. J. Weber. Effectiveness of  
544 ammonia reduction on control of fine particle nitrate, *Atmos. Chem. Phys.*, 18: 12241-56, 2018b
- 545 Guo, H., L. Xu, A. Bougiatioti, K. M. Cerully, S. L. Capps, J. R. Hite Jr, A. G. Carlton, S. H. Lee,  
546 M. H. Bergin, N. L. Ng, A. Nenes, and R. J. Weber. Fine-particle water and pH in the southeastern  
547 United States, *Atmos. Chem. Phys.*, 15: 5211-28, 2015
- 548 Guo, Hongyu, Amy P. Sullivan, Pedro Campuzano-Jost, Jason C. Schroder, Felipe D. Lopez-  
549 Hilfiker, Jack E. Dibb, Jose L. Jimenez, Joel A. Thornton, Steven S. Brown, Athanasios Nenes,  
550 and Rodney J. Weber. Fine particle pH and the partitioning of nitric acid during winter in the  
551 northeastern United States, *Journal of Geophysical Research: Atmospheres*, 121: 10,355-10,76,  
552 2016
- 553 Guo, Hongyu, Rodney J. Weber, and Athanasios Nenes. High levels of ammonia do not raise fine  
554 particle pH sufficiently to yield nitrogen oxide-dominated sulfate production, *Scientific Reports*,  
555 7: 12109, 2017
- 556 Gwynn, R. C., R. T. Burnett, and G. D. Thurston. A time-series analysis of acidic particulate matter  
557 and daily mortality and morbidity in the Buffalo, New York, region, *Environmental health*  
558 *perspectives*, 108: 125-33, 2000
- 559 Heim, E., J.E. Dibb, E. Scheuer, P. Campuzano-Jost, B.A. Nault, J.L. Jimenez, D. Peterson, C.  
560 Knote, M. Fenn, J. Hair, A.J. Beyersdorf, C. Corr, B.E. Anderson. Asian Dust Observed during  
561 KORUS-AQ Facilitates the Uptake and Incorporation of Soluble Pollutants during Transport to  
562 South Korea. *Atmos. Environ.*, in press, 2020
- 563 Hennigan, C. J., J. Izumi, A. P. Sullivan, R. J. Weber, and A. Nenes. A critical evaluation of proxy  
564 methods used to estimate the acidity of atmospheric particles, *Atmos. Chem. Phys.*, 15: 2775-90,  
565 2015
- 566 Hong, Jong Ho, Jitae Kim, Wonik Son, Heeyoung Shin, Nahyun Kim, Woong Ki Lee, and Jintae  
567 Kim. Long-term energy strategy scenarios for South Korea: Transition to a sustainable energy  
568 system, *Energy Policy*, 127: 425-37, 2019



- 569 Huebert, B. J., and C. H. Robert. The dry deposition of nitric acid to grass, *Journal of Geophysical*  
570 *Research: Atmospheres*, 90: 2085-90, 1985
- 571 Huey, L. G., D. J. Tanner, D. L. Slusher, J. E. Dibb, R. Arimoto, G. Chen, D. Davis, M. P. Buhr,  
572 J. B. Nowak, R. L. Mauldin, F. L. Eisele, and E. Kosciuch. CIMS measurements of HNO<sub>3</sub> and  
573 SO<sub>2</sub> at the South Pole during ISCAT 2000, *Atmospheric Environment*, 38: 5411-21 2004
- 574 Huey, L. Gregory, Peter W. Villalta, Edward J. Dunlea, David R. Hanson, and Carleton J. Howard.  
575 Reactions of CF<sub>3</sub>O- with Atmospheric Trace Gases, *The Journal of Physical Chemistry*, 100: 190-  
576 94, 1996
- 577 Huffman, J. A., K. S. Docherty, A. C. Aiken, M. J. Cubison, I. M. Ulbrich, P. F. DeCarlo, D.  
578 Sueper, J. T. Jayne, D. R. Worsnop, P. J. Ziemann, and J. L. Jimenez. Chemically-resolved aerosol  
579 volatility measurements from two megacity field studies, *Atmos. Chem. Phys.*, 9: 7161-82, 2009
- 580 Ito, T., Nenes, A., Johnson, M. S., Meskhidze, N., Valett, J., and Deutsch, C. Late 20th century  
581 deoxygenation of the tropical Pacific enhanced by aerosol pollutants, *Nature Geosci.*,  
582 doi:10.1038/ngeo2717, 2016
- 583 Jordan, Carolyn E. , James H. Crawford, Andreas J. Beyersdorf, Thomas F. Eck, Hannah S.  
584 Halliday, Benjamin A. Nault, Lim-Seok Chang, Rokjin Park, Gangwoong Lee, Hwajin Kim,  
585 Seogju Cho, Hye Jung Shin, Jae Hong Lee, Jinsang Jung, Deug-Soo Kim, Meehye Lee, Taehyoung  
586 Lee, Andrew Whitehill, James Szykman, Melinda Kaye Schueneman, Pedro Campuzano Jost, Jose  
587 L. Jimenez, Joshua P. DiGangi, Glenn S. Diskin, Bruce E. Anderson, Richard H. Moore, Luke D.  
588 Ziemba, Marta A. Fenn, Johnathan W. Hair, Ralph E. Kuehn, Robert E. Holz, Gao Chen, Katherine  
589 Travis, Michael Shook, David A. Peterson, Kara D. Lamb, Joshua P. Schwarz. Investigation of  
590 Factors Controlling PM<sub>2.5</sub> Variability across the South Korean peninsula during KORUS-AQ,  
591 *Elementa*, in review
- 592 Kafle, Sagar, Ranjan Parajuli, Sujala Bhattarai, Seung Hee Euh, and Dae Hyun Kim. A review on  
593 energy systems and GHG emissions reduction plan and policy of the Republic of Korea: Past,  
594 present, and future, *Renewable and Sustainable Energy Reviews*, 73: 1123-30, 2017
- 595 Kim, Minjoong J. Sensitivity of Nitrate Aerosol Production to Vehicular Emissions in an Urban  
596 Street, *Atmosphere*, 10: 212, 2019



- 597 Kim, Na Kyung, Yong Pyo Kim, Yu Morino, Jun-ichi Kurokawa, and Toshimasa Ohara.  
598 Verification of NO<sub>x</sub> emission inventory over South Korea using sectoral activity data and satellite  
599 observation of NO<sub>2</sub> vertical column densities, *Atmospheric Environment*, 77: 496-508, 2013
- 600 Kim, S., L. G. Huey, R. E. Stickel, D. J. Tanner, J. H. Crawford, J. R. Olson, G. Chen, W. H.  
601 Brune, X. Ren, R. Leshner, P. J. Wooldridge, T. H. Bertram, A. Perring, R. C. Cohen, B. L. Lefer,  
602 R. E. Shetter, M. Avery, G. Diskin, and I. Sokolik. Measurement of HO<sub>2</sub>NO<sub>2</sub> in the free  
603 troposphere during the Intercontinental Chemical Transport Experiment–North America 2004,  
604 *Journal of Geophysical Research: Atmospheres*, 112, 2007
- 605 Kim, H., Zhang, Q., and Heo, J.: Influence of intense secondary aerosol formation and long-range  
606 transport on aerosol chemistry and properties in the Seoul Metropolitan Area during spring time:  
607 results from KORUS-AQ, *Atmos. Chem. Phys.*, 18, 7149–7168, [https://doi.org/10.5194/acp-18-](https://doi.org/10.5194/acp-18-7149-2018)  
608 7149-2018, 2018
- 609 Kimmel, Joel R., Delphine K. Farmer, Michael J. Cubison, Donna Sueper, Christian Tanner, Eiko  
610 Nemitz, Douglas R. Worsnop, Marc Gonin, and Jose L. Jimenez. Real-time aerosol mass  
611 spectrometry with millisecond resolution, *International Journal of Mass Spectrometry*, 303: 15-26,  
612 2011
- 613 Koutrakis, Petros, Jack M. Wolfson, and John D. Spengler. An improved method for measuring  
614 aerosol strong acidity: Results from a nine-month study in St Louis, Missouri and Kingston,  
615 Tennessee, *Atmospheric Environment*, 22: 157-62, 1987
- 616 Lelieveld, J., J. S. Evans, M. Fnais, D. Giannadaki, and A. Pozzer. The contribution of outdoor air  
617 pollution sources to premature mortality on a global scale, *Nature*, 525: 367-71, 2015
- 618 Meskhidze, N., W. L. Chameides, A. Nenes, and G. Chen. Iron mobilization in mineral dust: Can  
619 anthropogenic SO<sub>2</sub> emissions affect ocean productivity?, *Geophysical Research Letters*, 30, 2003
- 620 Nakao, Motoyuki, Yoko Ishihara, Cheol-Hong Kim, and In-Gyu Hyun. The Impact of Air  
621 Pollution, Including Asian Sand Dust, on Respiratory Symptoms and Health-related Quality of  
622 Life in Outpatients With Chronic Respiratory Disease in Korea: A Panel Study, *Journal of*  
623 *preventive medicine and public health = Yebang Uihakhoe chi*, 51: 130-39, 2018
- 624 Nault, B. A., P. Campuzano-Jost, D. A. Day, J. C. Schroder, B. Anderson, A. J. Beyersdorf, D. R.  
625 Blake, W. H. Brune, Y. Choi, C. A. Corr, J. A. de Gouw, J. Dibb, J. P. DiGangi, G. S. Diskin, A.



- 626 Fried, L. G. Huey, M. J. Kim, C. J. Knote, K. D. Lamb, T. Lee, T. Park, S. E. Pusede, E. Scheuer,  
627 K. L. Thornhill, J. H. Woo, and J. L. Jimenez. Secondary organic aerosol production from local  
628 emissions dominates the organic aerosol budget over Seoul, South Korea, during KORUS-AQ,  
629 *Atmos. Chem. Phys.*, 18: 17769-800, 2018
- 630 Nenes, A., M. D. Krom, N. Mihalopoulos, P. Van Cappellen, Z. Shi, A. Bougiatioti, P. Zarmpas,  
631 and B. Herut. Atmospheric acidification of mineral aerosols: a source of bioavailable phosphorus  
632 for the oceans, *Atmos. Chem. Phys.*, 11: 6265-72, 2011
- 633 Nenes, A., Pandis, S. N., Weber, R. J., and Russell, A.: Aerosol pH and liquid water content  
634 determine when particulate matter is sensitive to ammonia and nitrate availability, *Atmos. Chem.*  
635 *Phys.*, 20, 3249–3258, <https://doi.org/10.5194/acp-20-3249-2020>, 2020a
- 636 Nenes, A., Pandis, S. N., Kanakidou, M., Russell, A., Song, S., Vasilakos, P., Weber, R. J.: Aerosol  
637 acidity and liquid water content regulate the dry deposition of inorganic reactive nitrogen, *Atmos.*  
638 *Chem. Phys. Disc.*, in review, 2020b
- 639 Osada, Kazuo. Measurements of Gaseous NH<sub>3</sub> and Particulate NH<sub>4</sub><sup>+</sup> in the Atmosphere by  
640 Fluorescent Detection after Continuous Air–water Droplet Sampling, *Aerosol and Air Quality*  
641 *Research*, 2011
- 642 Pozzer, A., A. P. Tsimpidi, V. A. Karydis, A. de Meij, and J. Lelieveld. Impact of agricultural  
643 emission reductions on fine-particulate matter and public health, *Atmos. Chem. Phys.*, 17: 12813-  
644 26, 2017
- 645 Pye, H. O. T., A. Nenes, B. Alexander, A. P. Ault, M. C. Barth, S. L. Clegg, J. L. Collett Jr, K. M.  
646 Fahey, C. J. Hennigan, H. Herrmann, M. Kanakidou, J. T. Kelly, I. T. Ku, V. F. McNeill, N.  
647 Riemer, T. Schaefer, G. Shi, A. Tilgner, J. T. Walker, T. Wang, R. Weber, J. Xing, R. A. Zaveri,  
648 and A. Zuend. The Acidity of Atmospheric Particles and Clouds, *Atmos. Chem. Phys.*, in press,  
649 2020
- 650 Raizenne, M., L. M. Neas, A. I. Damokosh, D. W. Dockery, J. D. Spengler, P. Koutrakis, J. H.  
651 Ware, and F. E. Speizer. Health effects of acid aerosols on North American children: pulmonary  
652 function, *Environmental health perspectives*, 104: 506-14, 1996
- 653 Riemer, N., Ault, A. P., West, M., Craig, R. L., & Curtis, J. H. Aerosol mixing state: Measurements,  
654 modeling, and impacts, *Reviews of Geophysics*, 57, 187–249, 2019



- 655 RSSR: Introduction to the KORUS-AQ Rapid Science Synthesis Report.  
656 <https://espo.nasa.gov/sites/default/files/documents/KORUS-AQ-ENG.pdf>, 2016
- 657 Saide, P. E., Gao, M., Lu, Z., Goldberg, D., Streets, D. G., Woo, J.-H., Beyersdorf, A., Corr, C.  
658 A., Thornhill, K. L., Anderson, B., Hair, J. W., Nehrir, A. R., Diskin, G. S., Jimenez, J. L., Nault,  
659 B. A., Campuzano-Jost, P., Dibb, J., Heim, E., Lamb, K. D., Schwarz, J. P., Perring, A. E., Kim,  
660 J., Choi, M., Holben, B., Pfister, G., Hodzic, A., Carmichael, G. R., Emmons, L., and Crawford,  
661 J. H. Understanding and improving model representation of aerosol optical properties for a Chinese  
662 haze event measured during KORUS-AQ, *Atmos. Chem. Phys. Discuss.*,  
663 <https://doi.org/10.5194/acp-2019-1022>, in review, 2019.
- 664 Schrader, F., and Brümmer., C. Land Use Specific Ammonia Deposition Velocities: a Review of  
665 Recent Studies (2004-2013), *Water, Air, and Soil Pollution*, 225: 2114-14, 2014
- 666 Seinfeld, J.H. and Pandis, S.N. *Atmospheric Chemistry and Physics: From Air Pollution to Climate*  
667 *Change*. John Wiley & Sons, Hoboken, 2016.
- 668 Shingler, T., Crosbie, E., Ortega, A., Shiraiwa, M., Zuend, A., Beyersdorf, A., Ziemba, L.,  
669 Anderson, B., Thornhill, L., Perring, A. E., Schwarz, J. P., Campuzano-Jost, P., Day, D. A.,  
670 Jimenez, J. L., Hair, J. W., Mikoviny, T., Wisthaler, A. and Sorooshian, A.: Airborne  
671 Characterization of Sub-saturated Aerosol Hygroscopicity and Dry Refractive Index from the  
672 Surface to 6.5 km during the SEAC 4 RS Campaign, *J. Geophys. Res. Atmos.*, 121(8), 4188–4210,  
673 doi:10.1002/2015JD024498, 2016
- 674 Slusher, Darlene L., L. Gregory Huey, David J. Tanner, Frank M. Flocke, and James M. Roberts.  
675 A thermal dissociation–chemical ionization mass spectrometry (TD-CIMS) technique for the  
676 simultaneous measurement of peroxyacyl nitrates and dinitrogen pentoxide, *Journal of*  
677 *Geophysical Research: Atmospheres*, 109, 2004
- 678 Song, S., M. Gao, W. Xu, J. Shao, G. Shi, S. Wang, Y. Wang, Y. Sun, and M. B. McElroy. Fine-  
679 particle pH for Beijing winter haze as inferred from different thermodynamic equilibrium models,  
680 *Atmos. Chem. Phys.*, 18: 7423-38, 2018
- 681 Song, S., M. Gao, W. Xu, Y. Sun, D. R. Worsnop, J. T. Jayne, Y. Zhang, L. Zhu, M. Li, Z. Zhou,  
682 C. Cheng, Y. Lv, Y. Wang, W. Peng, X. Xu, N. Lin, Y. Wang, S. Wang, J. W. Munger, D. J. Jacob,



- 683 and M. B. McElroy. Possible heterogeneous chemistry of hydroxymethanesulfonate (HMS) in  
684 northern China winter haze, *Atmos. Chem. Phys.*, 19: 1357-71, 2019
- 685 Tan, Tianyi, Min Hu, Mengren Li, Qingfeng Guo, Yusheng Wu, Xin Fang, Fangting Gu, Yu  
686 Wang, and Zhijun Wu. New insight into PM<sub>2.5</sub> pollution patterns in Beijing based on one-year  
687 measurement of chemical compositions, *Science of The Total Environment*, 621: 734-43, 2018
- 688 Thurston, G. D., K. Ito, C. G. Hayes, D. V. Bates, and M. Lippmann. Respiratory Hospital  
689 Admissions and Summertime Haze Air Pollution in Toronto, Ontario: Consideration of the Role  
690 of Acid Aerosols, *Environmental Research*, 65: 271-90, 1994
- 691 Vasilakos, P., A. Russell, R. Weber, and A. Nenes. Understanding nitrate formation in a world  
692 with less sulfate, *Atmos. Chem. Phys.*, 18: 12765-75, 2018
- 693 Wang, Haiting, Jing Ding, Jiao Xu, Jie Wen, Jianhong Han, Keling Wang, Guoliang Shi, Yinchang  
694 Feng, Cesunica E. Ivey, Yuhang Wang, Athanasios Nenes, Qianyu Zhao, and Armistead G.  
695 Russell. Aerosols in an arid environment: The role of aerosol water content, particulate acidity,  
696 precursors, and relative humidity on secondary inorganic aerosols, *Science of The Total  
697 Environment*, 646: 564-72, 2019
- 698 Wang, Shanshan, Jialiang Nan, Chanzhen Shi, Qingyan Fu, Song Gao, Dongfang Wang, Huxiong  
699 Cui, Alfonso Saiz-Lopez, and Bin Zhou. Atmospheric ammonia and its impacts on regional air  
700 quality over the megacity of Shanghai, China, *Scientific Reports*, 5: 15842, 2015
- 701 Warner, J. X., R. R. Dickerson, Z. Wei, L. L. Strow, Y. Wang, and Q. Liang. Increased atmospheric  
702 ammonia over the world's major agricultural areas detected from space, *Geophysical Research  
703 Letters*, 44: 2875-84., 2017
- 704 Womack, C. C., E. E. McDuffie, P. M. Edwards, R. Bares, J. A. de Gouw, K. S. Docherty, W. P.  
705 Dubé, D. L. Fibiger, A. Franchin, J. B. Gilman, L. Goldberger, B. H. Lee, J. C. Lin, R. Long, A.  
706 M. Middlebrook, D. B. Millet, A. Moravek, J. G. Murphy, P. K. Quinn, T. P. Riedel, J. M. Roberts,  
707 J. A. Thornton, L. C. Valin, P. R. Veres, A. R. Whitehill, R. J. Wild, C. Warneke, B. Yuan, M.  
708 Baasandorj, and S. S. Brown. An Odd Oxygen Framework for Wintertime Ammonium Nitrate  
709 Aerosol Pollution in Urban Areas: NO<sub>x</sub> and VOC Control as Mitigation Strategies, *Geophysical  
710 Research Letters*, 46: 4971-79, 2019



- 711 Xu, Z., M. Liu, Y. Song, S. Wang, L. Zhang, T. Xu, T. Wang, C. Yan, T. Zhou, Y. Sun, Y. Pan,  
712 m. Hu, M. Zheng, and T. Zhu, High efficiency of livestock ammonia emission controls on  
713 alleviating particulate nitrate during a severe winter haze episode in northern China, *Atm. Chem.*  
714 *Phys.*, 19, 5605-5613, 2019
- 715 Yokelson, R. J., T. J. Christian, I. T. Bertschi, and W. M. Hao. Evaluation of adsorption effects on  
716 measurements of ammonia, acetic acid, and methanol, *Journal of Geophysical Research:*  
717 *Atmospheres*, 108, 2003
- 718 Zhu, L., D. K. Henze, J. O. Bash, K. E. C.-P., M. W. Shephard, M. Luo, and S. L. Capps. Sources  
719 and Impacts of Atmospheric NH<sub>3</sub>: Current Understanding and Frontiers for Modeling,  
720 Measurements, and Remote Sensing in North America, *Current Pollution Reports*, 1: 95-116, 2015
- 721 Zhu, S., Sartelet, K.N., Zhang, Y., Nenes, A. Three-dimensional modelling of the mixing state of  
722 particles over Greater Paris, *J. Geoph.Res.*, 121, doi:10.1002/2015JD024241, 2016
- 723





724 **Table 1:** Summary of selected KORUS and other campaign data.

Campaign	KORUS-AQ	Institute of Urban Meteorology	SEARCH	CalNex	SOAS	SENEX
Type of Measurement	Air	Ground	Ground	Ground	Air	Air
Year	2016	2017	2010	2013	2013	2013
Season	Summer	Spring, Summer, Fall, Winter	Late Summer Early Fall	Summer	Summer	Summer
Location	South Korea	Beijing, China	SE U.S.	SW U.S.	SE U.S.	SE U.S.
Average RH (%)	62±12	-	69±18	79±17	74±16	72±9
Avg. HNO <sub>3</sub> (µg m <sup>-3</sup> )	4.61±2.72	-	0.50±0.26	6.65 ± 7.03	0.36 ± 0.14	1.35 ± 0.66
Avg. NO <sub>3</sub> concentration (µg m <sup>-3</sup> )	8.09± 6.16	12.6 ± 14.2 (spring), 13.7 ± 21.0 (winter), 9.5 ± 9.5 (summer), 18.5 ± 19.5 (fall)	0.2±0.1	PM1: 3.58 ± 3.65	0.08 ± 0.08	0.28 ± 0.09
Average ε(NO <sub>3</sub> )	58±24%	-	26±15%	39±16%	22±16%	18 ± 6 %
pH	2.43 ±0.68 (no NVCs) 2.45±0.96 (with NVCs)	4.3±1.6 (spring), 4.5±1.1 (winter), 3.9±1.3 (summer), 4.1±1.0 (fall)	2.2 ±0.6	1.9 ±0.5	0.9 ± 0.6	1.1 ± 0.4
Reference	This study	Ding et al. (2019)	Nah et al. (2018)	Guo et al. (2017)	Guo et al. (2015)	Xu et al. (2016)

725



726 **Figure Captions**

727 **Figure 1:** Average inorganic PM<sub>1</sub> mass composition throughout the entire study and for altitudes  
728 below 1km. Average total mass is 22 μg m<sup>-3</sup>.

729 **Figure 2:** Guo et al. (2016) method for constraining aerosol pH in the absence of NH<sub>3</sub> data.

730 **Figure 3:** Total ammonia (blue) and pH (red) as a function of iteration number using the Guo et  
731 al. (2016) algorithm.

732 **Figure 4:** The nitrate partitioning constrained pH (NPC-pH) method to obtain aerosol pH from  
733 nitrate partitioning observations.

734 **Figure 5:** Comparison of equilibrium nitrate partitioning retrieved from synthetic data vs. the  
735 value from the NPC-pH method. Meteorological conditions in the synthetic dataset cover a RH  
736 of 45-95%, Temperature 298K and SO<sub>4</sub>, NO<sub>3</sub><sup>T</sup>, NH<sub>4</sub><sup>T</sup> of 0.1-10 μg m<sup>-3</sup>, 0.2-110 μg m<sup>-3</sup>, and 0.2-  
737 110 μg m<sup>-3</sup>, respectively. Non-volatile cation concentrations were set to zero, and Cl-  
738 concentration was kept constant at 0.5 μg m<sup>-3</sup>.

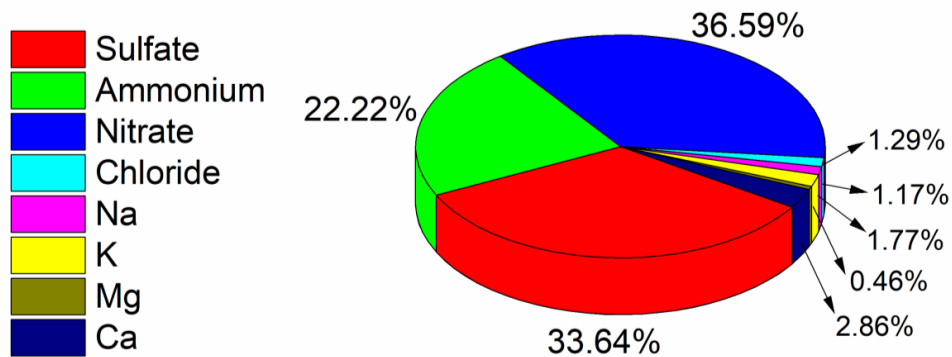
739 **Figure 6:** Particle phase fraction of total nitrate, ε(NO<sub>3</sub><sup>-</sup>) (blue curve) and total ammonium,  
740 ε(NH<sub>4</sub><sup>+</sup>) (red curve) versus pH for a temperature of 288 K and an aerosol liquid water content of  
741 10 μg m<sup>-3</sup>. The pink zone is a region where PM is sensitive to both HNO<sub>3</sub> and NH<sub>3</sub>. Following the  
742 approach of Nenes et al. (2020a), the dotted black line represents a pre-defined threshold, below  
743 which the aerosol is deemed insensitive to changes in NH<sub>3</sub> and/or HNO<sub>3</sub>.

744 **Figure 7:** (a) Flight trajectories for altitudes below 1km during KORUS-AQ, color mapped by  
745 NO<sub>3</sub><sup>-</sup> levels. Highest concentrations of NO<sub>3</sub><sup>-</sup> observed near Seoul, for which NO<sub>x</sub> emissions are  
746 dominated by the transportation and energy industries. (b) NO<sub>x</sub> emission sources in Korea labelled  
747 by industry.

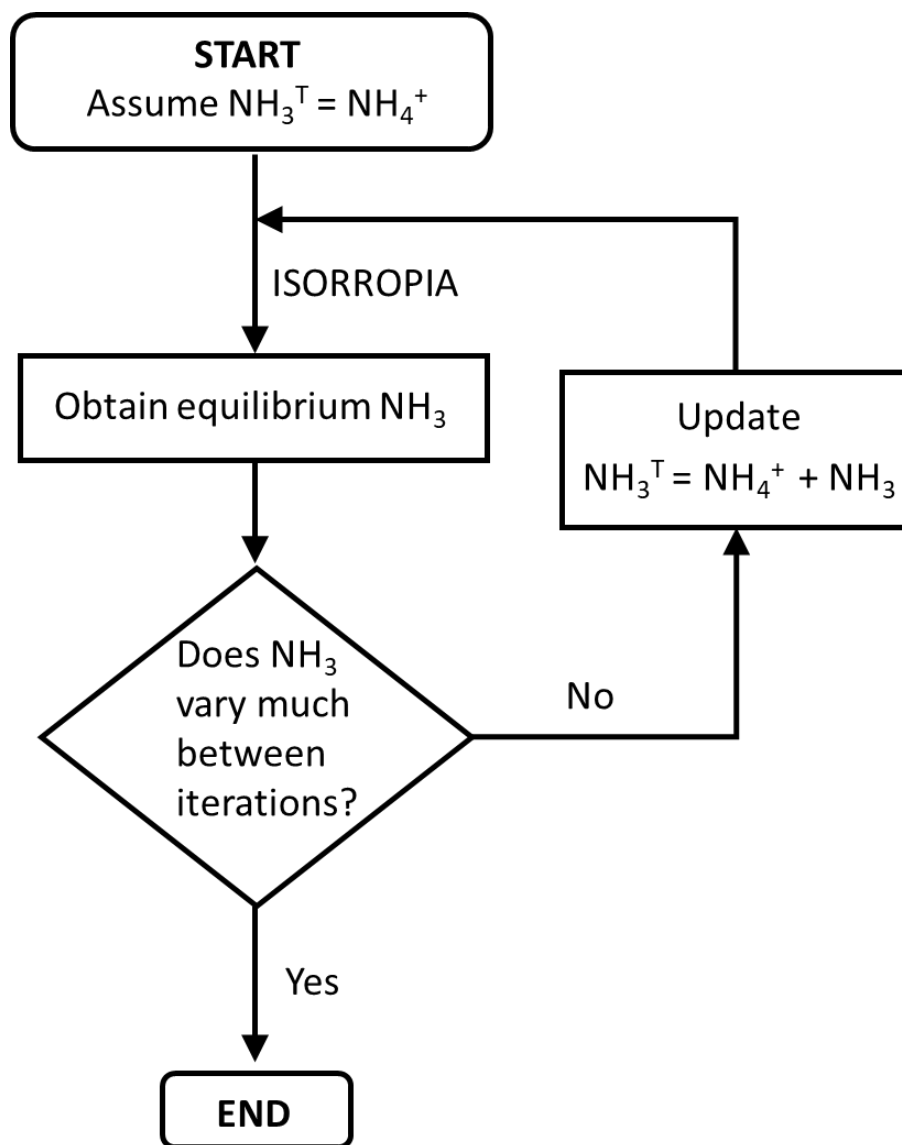
748 **Figure 8:** Chemical domains for entire KORUS-AQ study data. Larger fraction of data falls in  
749 HNO<sub>3</sub> sensitive region as a result of moderate-high values of nitrate partitioning.

750 **Figure 9:** Chemical domains for (a) flight 15 and (b) flight 19. For Flight 15, a significant  
751 number of its data points are characterized by low nitrate partitioning values (approx. 30%)<sup>\*\*</sup>.  
752 Flight 19 is characterized by high levels of particle nitrate, and moderate to high levels of nitrate  
753 partitioning. For these reasons, PM would be for response to NH<sub>3</sub> and HNO<sub>3</sub> for flights 15 and  
754 19 respectively.

755 **Figure 10:** Chemical domains for entire KORUS-AQ study data, with symbols colored by the  
756 value of PM.

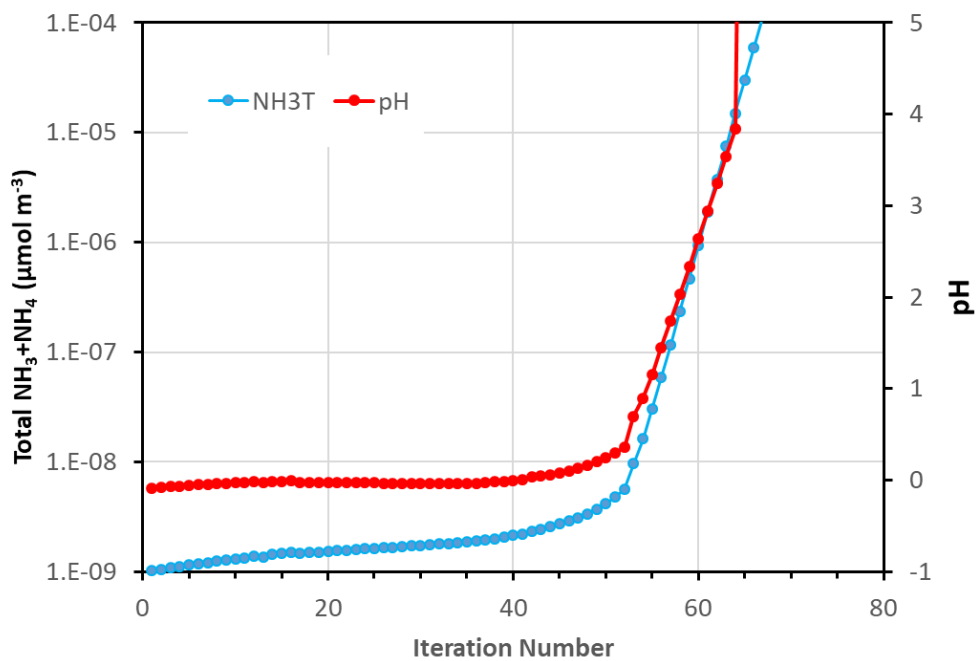


757  
758 **Figure 1**  
759  
760

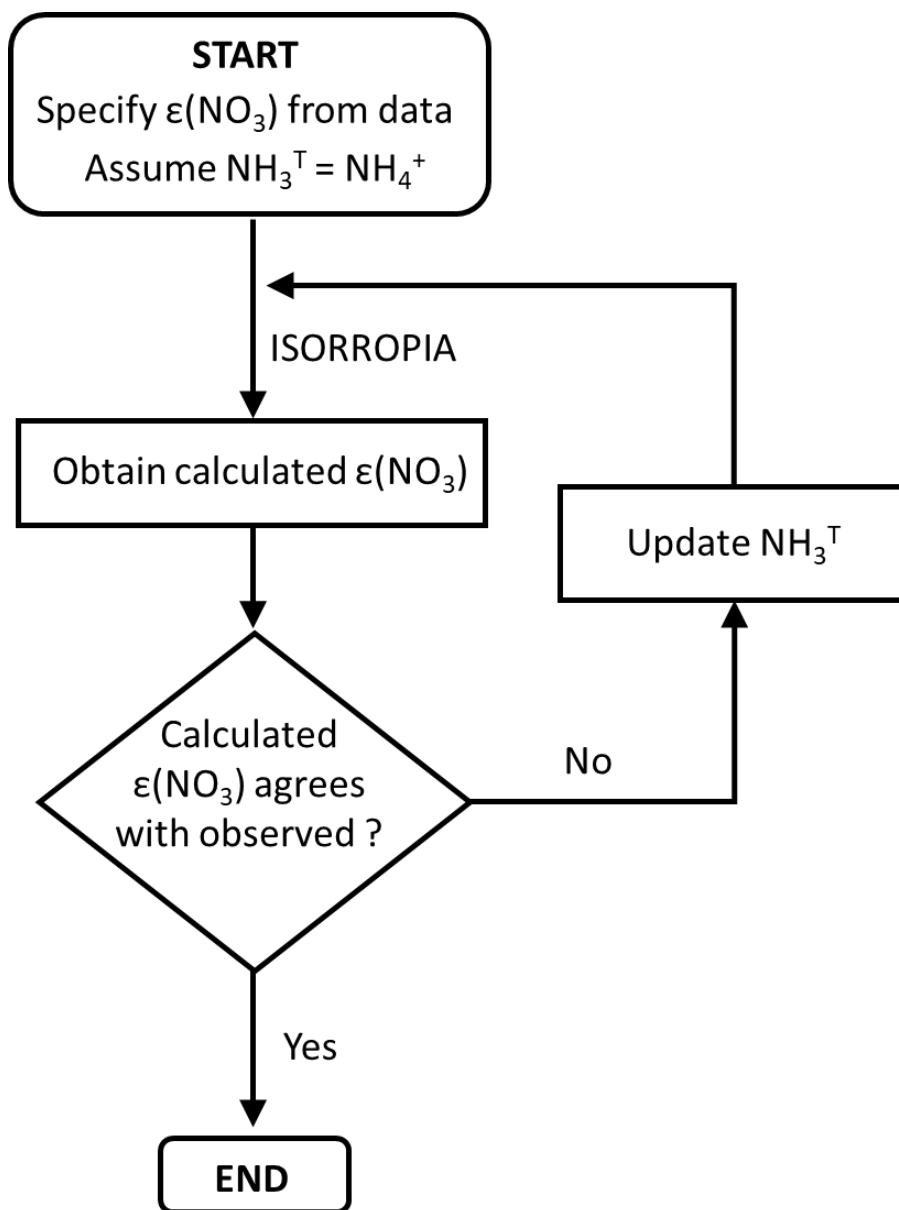


761  
762  
763

**Figure 2**

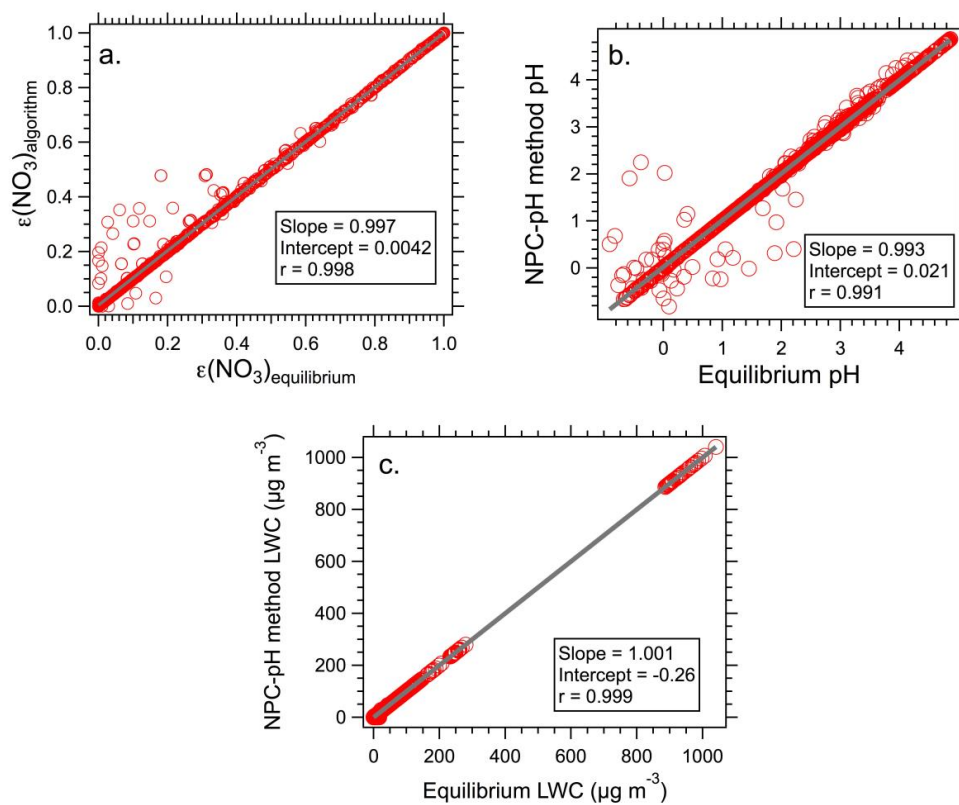


764  
765 **Figure 3**  
766



767  
768  
769  
770

Figure 4

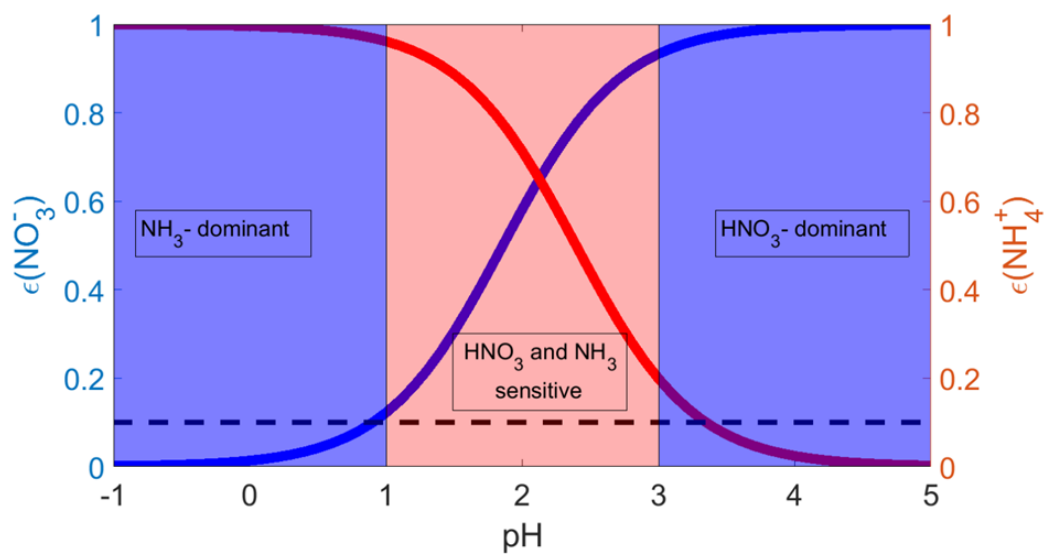


771  
772  
773  
774

**Figure 5**



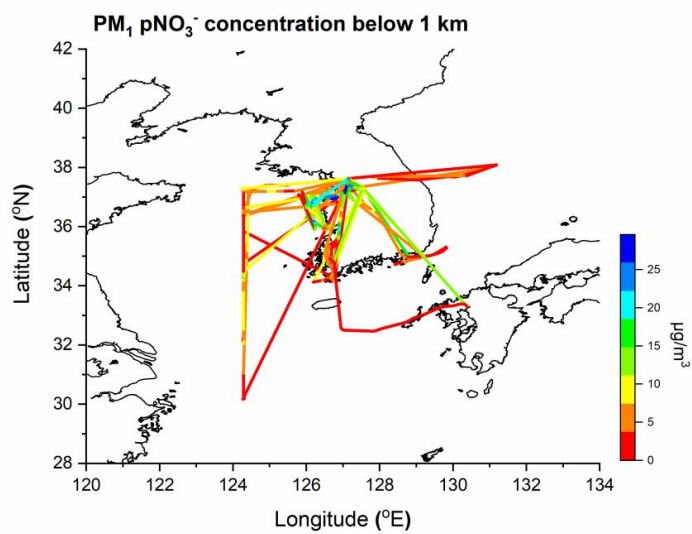
775



776  
777  
778

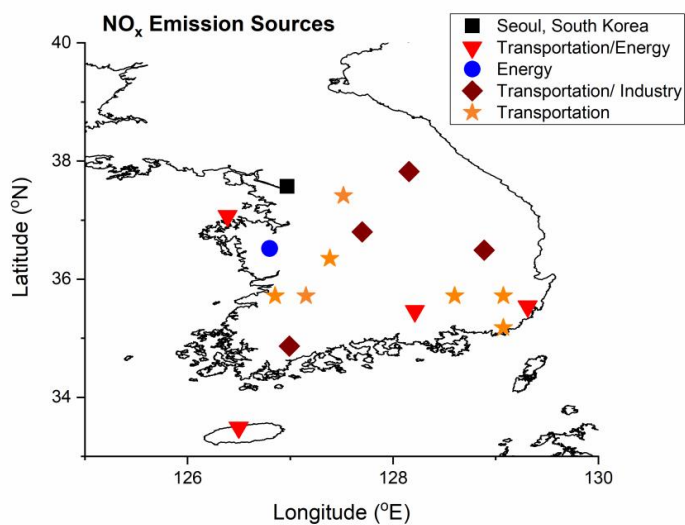
Figure 6





779  
780  
781

(a)



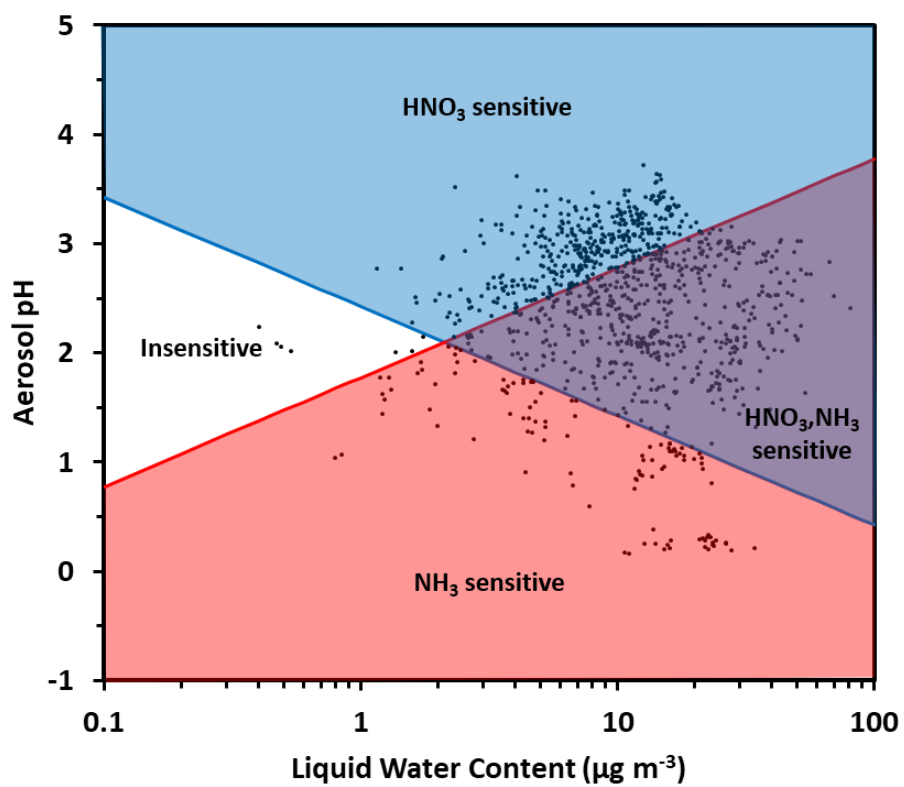
782  
783  
784  
785  
786

(b)

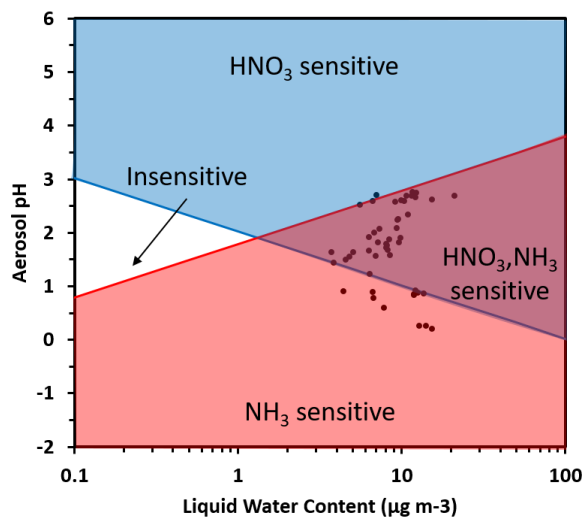
**Figure 7**



787

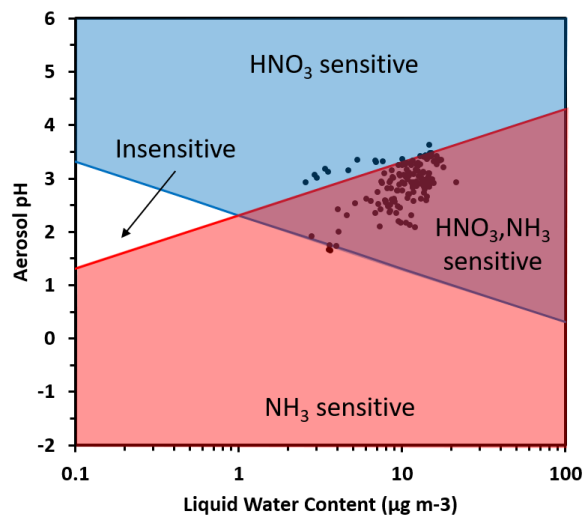


788  
789 **Figure 8**  
790  
791  
792  
793



794  
795  
796

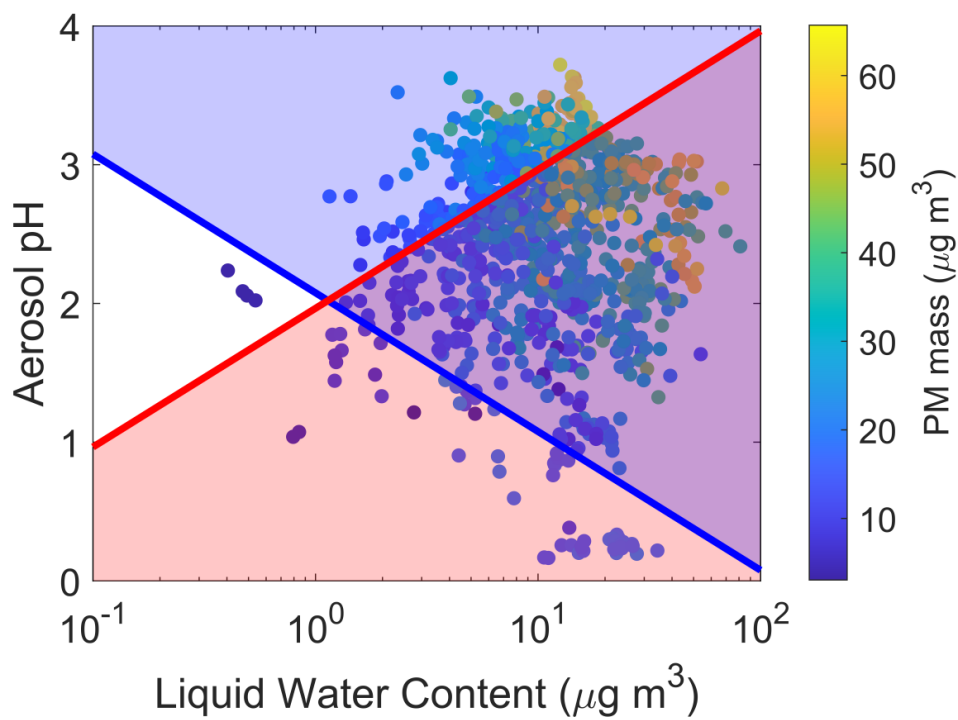
(a)



797  
798  
799  
800

**Figure 9**

(b)



801  
802  
803  
804  
805

**Figure 10**